

THERMAL PERTURBATIONS BENEATH THE INCIPIENT OKAVANGO RIFT
ZONE, NORTHWEST BOTSWANA

By

KHUMO LESEANE

Bachelor of Science in Geology
University of Botswana
Gaborone, Botswana
2009

Submitted to the Faculty of the
Graduate College of the
Oklahoma State University
in partial fulfillment of
the requirements for
the Degree of
MASTER OF SCIENCE
May, 2014

THERMAL PERTURBATIONS BENEATH THE INCIPIENT OKAVANGO RIFT
ZONE, NORTHWEST BOTSWANA

Thesis Approved:

Dr. Estella A. Atekwana

Thesis Adviser

Dr. Mohamed G. Abdelsalam

Dr. Eliot A. Atekwana

ACKNOWLEDGEMENTS

This research was made possible by my professor, advisor, and committee chair, Dr. Estella Atekwana of Oklahoma State University (OSU). I am also appreciative of my other committee members, Dr. Mohamed Abdelsalam and Dr. Eliot Atekwana for their ideas and recommendation in refining my work. Furthermore, I would like to thank Dr. Kevin Mickus of Missouri State University (MSU) for assisting me with fieldwork and providing the inversion codes for the three dimensional inversion components of my thesis. I also appreciate Kitso Matende, Kyle Obenberger and Galaletsang Motseokae for field assistance. Thanks to big brother Andrew Katumwehe for his mentorship and the long hours in NRC 203B.

This project is funded by the National Science Foundation – Continental Dynamics grant # EAR 1255233. I would like to extend special thanks to the Geological Survey of Botswana for allowing us free access to the airborne magnetic data and Bouguer gravity anomaly data for our study. My sincerest gratitude also goes to the University of Botswana for providing our research team with logistical support while conducting field work in Botswana.

I would like to thank Oklahoma State University and the Boone Pickens's School of Geology for providing me with quality education and skills that has prepared me for my future. I am grateful for all of the scholarships, especially the Alumni Graduate

Fellowship, which assisted me in pursuing my education. My special thanks to all the professors who helped me as a graduate student. I appreciate all of my friends and geology family that welcomed me to OSU and continued to encourage me and make me feel at home during my studies at OSU.

I am thankful to my mother (Bale Leseane) and my siblings (especially my triplet sister and brother) for being a permanent and consistent source of encouragement and support. Thank you for your unconditional support and guidance.

Acknowledgements reflect the views of the author and are not endorsed by committee members or Oklahoma State University.

Name: KHUMO LESEANE

Date of Degree: MAY, 2014

Title of Study: THERMAL PERTURBATIONS BENEATH THE INCIPIENT
OKAVANGO RIFT ZONE, NORTHWEST BOTSWANA

Major Field: GEOLOGY

Abstract:

We use aeromagnetic and Bouguer gravity data from the incipient Okavango Rift Zone (ORZ), the surrounding Archean cratons and Proterozoic mobile belts in northwestern Botswana to estimate the depth to the Curie isotherm and the crustal thickness beneath the rift. Imaging the depth to the base of magnetic sources is important in understanding and in constraining the thermal structure of the continental crust in zones of incipient continental rifting where no other data are available to image the crustal thermal structure. Our objective was to determine if there are thermal perturbations within the lithosphere under this young rift that might be suggestive of the presence of magmatic processes associated with rift initiation. The top and bottom of the magnetized crust were calculated using the two dimensional (2D) power-density spectrum analyses and three dimensional (3D) inversion of the total field magnetic data in overlapping windows of $1^\circ \times 1^\circ$. We found out that the Curie Point Depth (CPD) estimates vary between ~7 and ~23 km. The deepest CPD values (16 to 23 km) occur within the cratons which have lithospheric thickness greater than 200 km. Within the orogenic mobile belts, the CPD estimates range between 15 and 17 km. The shallowest CPD values of 7 – 14 km occur beneath the ORZ. In the northeastern part of ORZ with more developed rift structures, hot springs are known to occur. The shallowest CPD values, high heat flow and thin crust occur within a zone of ~60 km along the southeastern boundary of the ORZ and coincide with a strong NE-trending basement fabric, possibly acting as conduits for upward migration of hot fluids. These observations suggest the existence of a possible thermal anomaly within the lithosphere at shallow crustal depths beneath ORZ. We interpret the thermal anomaly as resulting from an infiltration front of melts/fluids due to ascending asthenosphere. Additional detailed tomographic imaging to be obtained as part of the Project for Rift Initiation, Development and Evolution experiments is needed to confirm this proposition.

TABLE OF CONTENTS

Chapter	Page
I. INTRODUCTION	1
II. REGIONAL GEOLOGIC AND TECTONIC SETTING	6
III. THE OKAVANGO RIFT ZONE	9
IV. METHODOLOGY	14
4.1 <i>Curie point depth analysis (CPD)</i>	14
4.1.1 <i>Two-dimensional radial power density spectral analysis</i>	14
4.1.2 <i>Three dimensional inversions</i>	19
4.2 <i>Heat flow estimates from CPD</i>	21
4.3 <i>Crustal thickness (Moho depth)</i>	22
V. RESULTS	26
5.1 <i>Curie Point Depth (CPD)</i>	26
5.2 <i>Heat Flow</i>	29
5.3 <i>Crustal thickness (Moho depth)</i>	31
VI. DISCUSSION.....	33
6.1 <i>Thermal structure beneath the ORZ and surrounding cratons and orogenic belts</i>	33
6.2 <i>Moho structure and thermal perturbations</i>	36
6.3 <i>Pre-existing structures and thermal perturbation</i>	39
6.4 <i>Source of thermal anomalies below the ORZ</i>	39
VII. CONCLUSION	43
VIII. FUTURE WORK.....	45
REFERENCES	47
APPENDICES	53

LIST OF FIGURES

Figure	Page
1. Digital Elevation Models (DEMs) extracted from the Global 30 Arc Second Elevation Data (GTOPO30, 1 km spatial resolution) showing the different parts of the Southwestern Branch of the East African Rift System. A=Afar. MER=Main Ethiopian Rift. R. Rhino graben. AL=Albertine graben. TA=Tarkana rift. TD=Tanzania divergence. K. Kivu rift. T=Tanganyika rift. RU=Rukwa rift. M=Mweru rift. L=Luangwa rift. MA=Malawi rift. D=Dombe rift. ORZ=Okavango rift zone. DGC=Damara-Ghanzi-Chobe orogenic belt.	8
2. Geological map of the Okavango Rift Zone showing the major faults and sub-basins of the rift. The rift is characterized by three sub-basins: Ngami, Mababe and Linyanti-Chobe sub-basins (After Mosley-Bufford et al., 2012)	13
3. The aeromagnetic map of the Okavango Rift Zone. The NE-trending magnetic anomalies are the result of regional foliation and folding within the Damara-Ghanzi-Chobe belt. The NW-trending magnetic anomalies represent the Okavango Dike Swarm. The profile A-B is the location of the of the cross-section presented in Figure 5b	15
4. (a) An example of the 2D power-density spectrum analyses used for the computation of the top of the magnetic source (Z_t) values using the relationship $(\ln [\Phi\Delta T (k)^{1/2}])$ and the lower wavelength number of 0.5-0.8 rad/km. (b) An example of the 2D power-density spectrum analyses used for the computation of the centroid (Z_c) using the relationship $(\ln [\Phi\Delta T (k)^{1/2}/ k])$ and the high wavenumber of 0.02-0.3 rad/km $\Phi\Delta T$ is the radial power density spectrum of the total magnetic field and K is the wave number. The CPD is calculated by using the relationship ($Z_b = 2Z_c - Z_t$). In this case $Z_b = 2 \times 10 \text{ km} - 6.67 \text{ km}$; $Z_b = 13.33 \text{ km}$	18
5. (a) An example of $1^\circ \times 1^\circ$ sub-block with ~40 depth and E-W depth slices (labeled a, b, c, d, and e) illustrating the 3D inversion of the aeromagnetic data used for the calculation of Curie Point Depth. The sub-block is from the southwestern part of the Okavango Rift Zone. (b) 3D inversion cross-section along a NW-SE profile showing the distribution of magnetization beneath the Okavango Rift Zone and surrounding terrains. GF= Gumare Fault. TF= Tsau Fault. ThF= Thamalakane Fault. KSZ= Kalahari Suture Zone. The pink and red lines are the approximate base of magnetization and Moho depth respectively	20

Figure	Page
6. The Bouguer anomaly map used for estimating the crustal thickness in northern Botswana through the 2D power-density spectrum analyses. The profile A-B is the location of the cross-section presented in Figure 10.....	24
7. An example of the 2D power-density spectrum analysis curve used for the estimation of the crustal thickness values. The radial power spectrum is plotted against the wavenumber and a series of points which are represented by one or more straight lines in Layer 2 on the graph are used to calculate the crustal thickness.....	25
8. Curie Point Depth values in kilometers obtained from the 3D inversion method for the Okavango Rift Zone (ORZ) and surrounding. The black star is the hot spring with temperature of 43 °C. The hatched lines are normal faults. ORZ=Okavango Rift Zone.	28
9. Map of heat flow values in mWm ² calculated using Curie point depth from 3D inversion results. The red circles are heat flow values from borehole measurement by Ballard et al. [1987]. The black star is the hot spring with temperature of 43 °C. The hatched lines are normal faults. ORZ; Okavango Rift zone	30
10. A schematic NW-SE cross-section along profile A-B shown in Figure 3 and 6 illustrating the lithosphere and thermal structure of the Okavango Rift Zone. The shallow Curie Point Depth (CPD), Moho, and elevated lithosphere/ asthenosphere boundary as found under the rift	37

LIST OF TABLES

Table	Page
Table 1. Crustal thickness estimation from gravity compared to data from passive seismic stations in eastern Botswana from the Kaapvaal project	31

CHAPTER I

INTRODUCTION

Numerical models for explaining continental rifting highlight the importance of magma in softening the lithosphere and enhancing lithospheric stretching [Buck, 2006]. Buck [2006] suggested that continuous intrusion of dikes thermally weakens the lithosphere, therefore reducing the amount of driving force needed to nucleate rifting. In these models, extensional strain is localized and maintained through magma intrusions. Such magma-assisted rifting models have been validated in the more developed segments of the East African Rift System (EARS) such as the Afar Depression and the Main Ethiopian Rift (Figure 1) [Ebinger and Casey, 2001; Ebinger, 2005; Kendall et al., 2005].

The role of magma in the initiation of rifting along the Western and Southwestern Branches of the EARS (Figure 1) has not been fully validated. The Western and Southwestern Branches are considered to be amagmatic. Different from rifts in other parts of the EARS, no volcanic centers are found within these branches other than sparse volcanic rocks found at the tips of individual basins within accommodation zones [Ebinger and Casey, 2001]. For example, within the southern termination of the EARS, basins such as the Malawi rift (Figure 1) show typical structural features associated with

ripping but there is no observed surface magmatism [Chorowicz, 2005]. For most of these rifts, extension is localized within Proterozoic orogenic belts, which circumscribe craton boundaries [Chorowicz, 2005; Begg et al., 2009; Craig et al., 2011], highlighting the important role that lithospheric heterogeneities and variations in lithospheric thickness play in the localization of strain during early stages of continental extension.

The Ethiopian part of the EARS is considered a type-locality example of magma-assisted rifting due to extensive magmatism associated with the extensional structures. Passive seismic results from the Main Ethiopian Rift and the Afar Depression confirm the existence of slower P and S-wave velocities suggestive of asthenospheric upwelling beneath the rifts [e.g., Maguire et al., 2006; Bastow et al., 2008; Keranen et al., 2009; Mulibo and Nyblade, 2013]. Additionally, the presence of shallow conductors imaged by Magnetotelluric (MT) method confirmed the presence of partial melts beneath these rifts [Whaler and Hautot, 2006]. Similar results have been observed beneath the Rio Grande Rift from EarthScope MT imaging found strong conductors in the lower crust at ~20 km depth comparable to conductivities observed in other tectonically-active areas around the world [Feucht et al., 2013; Jones et al., 2013]. Our current understanding and models of geodynamic processes explaining rift initiation are therefore strongly influenced by observations from the more evolved rift systems.

Estimates of the lithospheric thickness in the southern part of Africa suggest the presence of cratons with thick roots (over 200 km thick) and orogenic belts with

relatively thinner lithosphere (~100 km average) [Begg et al., 2009; Craig et al., 2011; Khoza et al., 2013]. Models such as small-scale mantle convection have been used to explain rift initiation in this type of tectonic setting where edge-driven mantle convection is induced by lateral thermal gradients resulting from the differences in the lithospheric thickness [van Wijk et al., 2008; Levander and Miller, 2012]. The edge-driven mantle convection model predicts a pattern of convectional cells with downward-directed flow under the thick lithosphere of the craton and upward-directed flow under the thinner lithosphere of the orogenic belt [van Wijk et al., 2008]. This model has been used to explain the onset of the Rio Grande Rift in the western US [van Wijk et al., 2008]. East of the Rio Grande Rift, the lithosphere of the western Great Plains extends to a depth of 150-180 km whereas the lithosphere under the Colorado plateau might have been only ~120 km thick [van Wijk et al., 2008]. The observations from the Rio Grande Rift prompt consideration of the fact that variations in the lithospheric thickness might have played an important role in the initiation of rifting in the amagmatic segments of the EARS.

Our understanding of the initiation processes within amagmatic rift zones is limited due to the paucity of geophysical observations of the crust and upper mantle underlying these structures. Within amagmatic, surface magmatism is often missing despite the presence of diagnostic rift features such as well-developed border faults and deep asymmetric grabens [Chorowicz, 2005], thereby calling into question the necessity of magmatism in rift initiation. There is a need therefore to consider alternative geodynamic processes responsible for amagmatic rift initiation. A new project

abbreviated as Project for Rift Initiation Development and Evolution (PRIDE) is anticipated to close this knowledge gap. PRIDE will provide the geophysical imaging beneath nascent rift segments of the EARS such as Malawi and Okavango, hence providing a missing snapshot in the study of continental rift systems.

The thermal structure of the lithosphere controls the modes of extension, depth extent of brittle or ductile behavior of the lithosphere and more importantly, the regional heat flow variations within areas of extension [Dolmaz et al., 2005]. Hence, the thermal structure beneath incipient rift zone is an important parameter that could be used to understand and constrain mechanisms responsible for strain localization during onset of rifting.

Typically, heat flow measurements obtained from boreholes and deep mines provide direct assessment of the thermal structure of the lithosphere [Hussein et al., 2012].

Although reliable, the sparse distribution of boreholes and their limited depth restricts mapping the thermal structure of the lithosphere to only low horizontal spatial resolution and a few kilometers depth [Hussein et al., 2012]. Alternatively, estimates of the temperature variations of the lithosphere can be obtained from helium isotopes measured in thermal springs, silica thermometry of thermal waters, MT method, seismic velocities, or magnetic data using two dimensional (2D) power-density spectrum analyses and three dimensional (3D) inversion.

The use of magnetic data to estimate the Curie point isotherm was first suggested by Bhattacharyya [1964] and subsequently improved by Spector and Grant [1970],

Bhattacharyya and Leu [1975], Tanaka et al. [1999] and references therein. The Curie point is the temperature at which spontaneous magnetization is lost and magnetic minerals become paramagnetic (magnetite ~580 °C) at atmospheric pressure. The depth to the bottom of the magnetized crust is directly related to the Curie isotherm and the variation in this depth reflects variation in the temperature of the crust [Aboud et al., 2011].

A major problem in understanding the thermal structure of the ORZ is that direct heat flow measurements are from sparsely-distributed boreholes [Ballard et al., 1987]. Hence, the thermal structure of this nascent rift remains poorly constrained, hindering the evaluation of lithospheric thermal perturbation as a mechanism for strain localization during the onset of continental rifting. In this paper, we used 2D power-density spectrum analyses and 3D inversion of aeromagnetic data to investigate the thermal structure of the crust under the incipient Okavango Rift Zone (ORZ) and the surrounding cratons and orogenic belts. The ORZ represents the youngest segment of the EARS and serves as an ideal laboratory for testing the role of thermal perturbation during initial stages of rifting.

CHAPTER II

REGIONAL GEOLOGIC AND TECTONIC SETTING

The EARS is a classic example of a continental rift zone [Chorowicz, 2005]. Generally, the surface morphology of the EARS is made-up of several discrete and diachronous fault-controlled rift basins, with or without surface extension of volcanic rocks [Ebinger, 2005]. Other features include along-strike segmentation defined by asymmetric basins bounded by en-echelon or curvilinear border faults with high relief [Chorowicz, 2005]. The EARS is divided into the Eastern, Western and Southwestern Branches (Figure 1). The Eastern Branch of the rift system extends from the Afar depression in Ethiopia and includes the Main Ethiopian Rift in the north and passes through the Turkana rift and the Tanzanian divergent zone in the central Tanzania and propagates down to the south. Further south, it becomes more diffuse as the rift encounters the thick lithosphere of the Tanzanian craton [Craig et al., 2011]. Rifting along the Eastern Branch is postulated to have been initiated at ~25 Ma [Roberts et al., 2012]. Roberts et al. [2012] suggests that the Eastern Branch was well-developed by 20 Ma]. The younger (<15 Ma), less-developed and amagmatic Western Branch constitutes segmented rift basins that include from the north to south: Albertine-Rhino, Kivu,

Tanganyika, Rukwa and Malawi (Figure 1). Further south, the Western Branch terminates in the Dombe and Urema half-grabens in Mozambique (Figure 1) [Kampunzu et al., 1998].

The Southwestern Branch of the EARS extends within southeastern Congo, southeastern Zambia, northeastern Zimbabwe and northeastern Botswana (Figure 1) [Reeves, 1972; Scholz et al., 1976; Ballard et al., 1987; Modisi et al., 2000; Kinabo et al., 2007; 2008; Mosley-Bufford et al., 2012 and references there in]. It forms a ~250 km wide zone of extension stretching for ~1700 km in a southwestern direction [Modisi et al., 2000]. It consists of a series of ~100 km long and 40-80 km wide Quaternary rift basins. These include the Mweru rift that extends southwest of the Tanganyika rift and the Luangwa rift which extends southwest of the Malawi rift and ultimately into the ORZ (Figure 1)[Modisi et al., 2000; Kinabo et al., 2008; Mosley-Bufford et al., 2012].

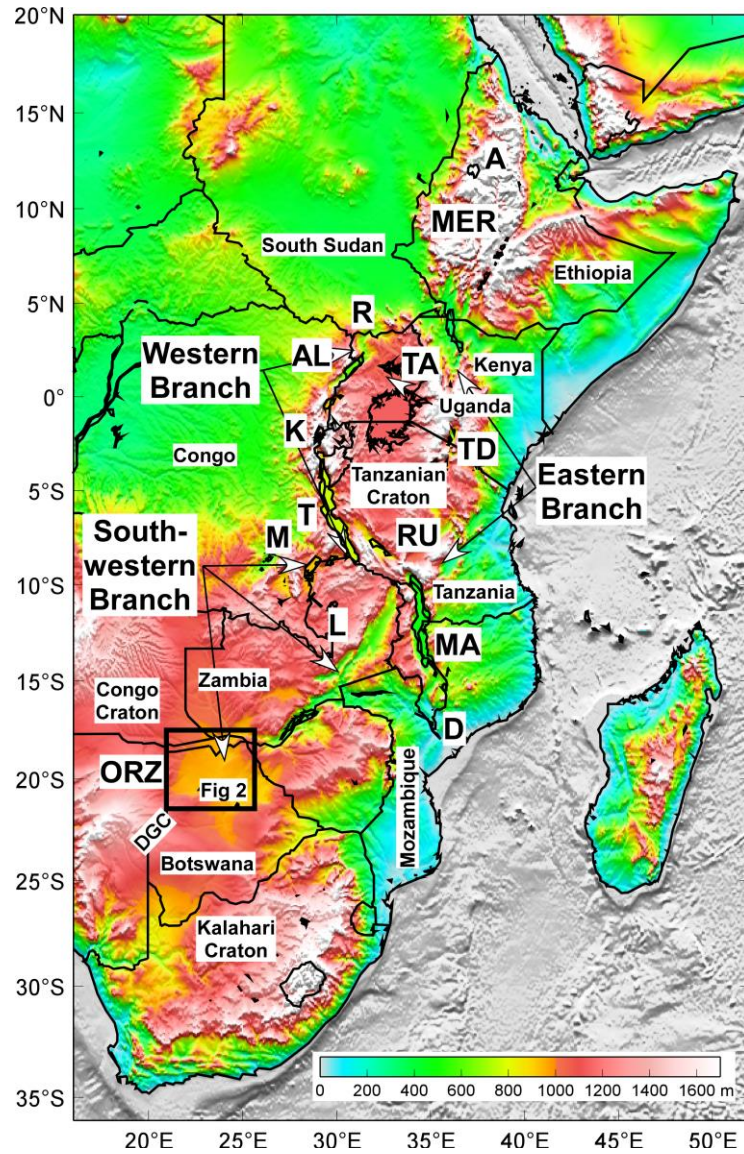


Figure 1. Digital Elevation Models (DEMs) extracted from the Global 30 Arc Second Elevation Data (GTOPO30, 1 km spatial resolution) showing the different parts of the Southwestern Branch of the East African Rift System. A=Afar. MER=Main Ethiopian Rift. R. Rhino graben. AL=Albertine graben. TA=Tarkana rift. TD=Tanzania divergence. K. Kivu rift. T=Tanganyika rift. RU=Rukwa rift. M=Mweru rift. L=Luangwa rift. MA=Malawi rift. D=Dombe rift. ORZ=Okavango rift zone. DGC=Damara-Ghanzi-Chobe orogenic belt.

CHAPTER III

OKAVANGO RIFT ZONE

The ORZ (Figure 2) is developing within the Proterozoic Damara-Ghanzi-Chobe orogenic belt, sandwiched between the Archean Congo craton in the northwest and the Archean Kalahari craton to the southeast (Figure 1) [Modisi et al., 2000; Kinabo et al., 2007; 2008]. The Damara-Ghanzi-Chobe orogenic belt is characterized by NE-trending fabric associated with the NE-striking folds and faults [Modisi et al., 2000; Kinabo et al., 2008; Mosley-Bufford et al., 2012]. This orogenic belt is partially covered by unconsolidated Quaternary sediment of the Kalahari alluvium and Holocene lacustrine sediments within paleo-lakes [Ringrose et al., 2005].

The ORZ has been the focus of surface and subsurface geologic and geophysical investigations aimed at determining its geometry and deciphering the nature and kinematics of the associated faults [Scholz et al., 1976; Modisi et al., 2000; Kinabo et al., 2008; Mosley-Bufford et al., 2012; Khoza et al., 2013]. Passive seismic investigations have focused on resolving the focal mechanisms associated with rift faulting [Reeves 1972; Scholz et al., 1976 and references there in]. Scholz et al. [1976] suggested from passive seismic results that the EARS extend to the southwest into northwestern

Botswana. Scholz et al. [1976] determined the focal mechanisms of the NE-trending faults of the ORZ to indicate normal faulting within a 150 km wide graben. Furthermore, Modisi et al. [2000] analyzed aeromagnetic data and postulated that the faults within the ORZ are normal faults that exploited pre-existing zones of weaknesses in the Precambrian basement. Kinabo et al. [2008] integrated Shuttle Radar Topography Mission (SRTM) Digital Elevation Models (DEM) and aeromagnetic data to reveal the fault development pattern and suggested that although the width of the ORZ is approximately 150 km, most of the faulting is occurring within ~60 km wide graben in the southeastern margin of the rift. Within the ORZ the fault, growth and propagation is occurring through both soft linkages and hard linkages and the border fault system is still developing and occurring by fault piracy [Kinabo et al., 2007; 2008].

Shallow MT and 2D inversion of direct current electrical resistivity results were used to suggest that the ORZ is an asymmetrical half-graben with the main NE-trending border fault occurring in the southeastern side of the rift [Mosley-Bufford et al., 2012]. The presence of fluids acts as lubricants promoting micro-seismicity [Mosley-Bufford et al., 2012].

The ORZ contains three areas of maximum sedimentary deposition constituting individual sub-basins in the southeastern margin of the rift. These are the Ngami sub-basin, the Mababe and the Linyanti-Chobe sub-basin (Figure 2). The Linyanti-Chobe sub-basin is found in the northeastern part of the ORZ bounded by the Linyanti fault in

the northwest and the Chobe fault to the southeast (Figure 2). To the southwest the Mababe sub-basin is bounded by the Chobe fault in the northwest and the Mababe fault to the southeast. Further to the southeast, the Ngami sub-basin is bounded by the Tsau fault in the northwest and the Kunyere fault to the southeast [Modisi et al., 2000; Kinabo et al., 2008; Mosley-Bufford et al., 2012]. The sedimentary thicknesses within the Ngami and Mababe sub-basins are estimated to be between 400 and 800 meters respectively [Kinabo et al., 2007; Shemang and Molwalefhe, 2009].

Results from MT surveys along regional profiles carried out as part of the Southern African Magnetotelluric Experiment (SAMTEX) provided the first lithospheric-scale electrical imaging beneath the ORZ. The SAMTEX experiment results suggest variations in the thickness of the lithosphere from the cratons to the orogenic belts, with thicker lithospheric keels (~180-250 km) beneath the Congo and Kalahari cratons compared to a thinner (~160 km) lithosphere beneath the Damara-Ghanzi-Chobe orogenic belt [Muller et al. 2009; Miensoopust et al., 2013; Khoza et al., 2013].

The onset of rifting in the ORZ has been suggested from studies using palaeo-environmental reconstruction from sediments and surface expression of features such as sand dunes and diversion of major drainage patterns. Using the Kalahari sand dunes offset, Scholz et al. [1976] suggested that rifting started in the Holocene. Moore and Larkin [2001] correlated the impoundment of the Okavango River (Figure 2) and change in drainage patterns with major uplift along the Zimbabwe-Kalahari axis and

displacement on the NE-trending faults of the ORZ, and suggested that rifting initiated between ~120 Ka and ~40 Ka. This is supported by geochemical and isotopic evidence from sediments collected in the Mababe sub-basin [Gamrod, 2009].

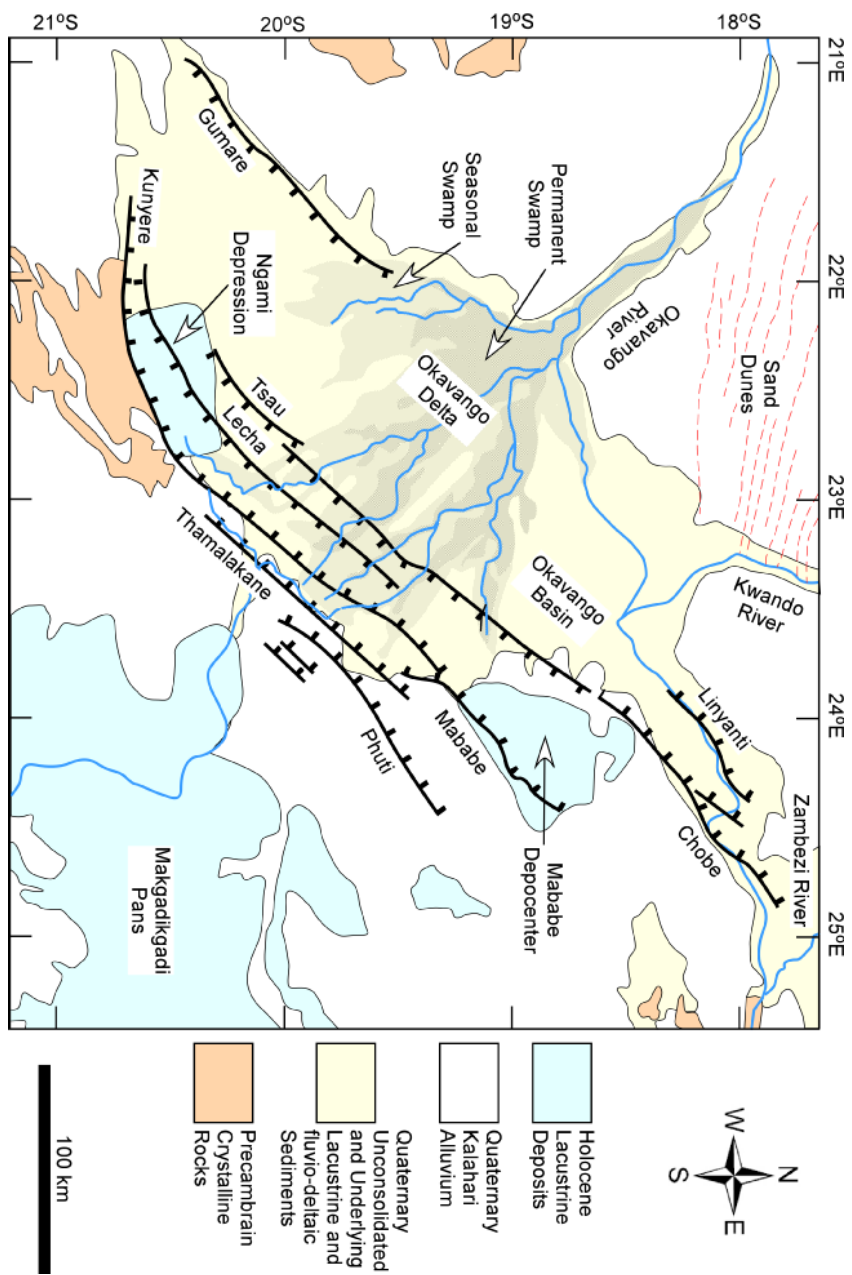


Figure 2. Geological map of the Okavango Rift Zone showing the major faults and sub-basins of the rift. The rift is characterized by three sub-basins: Ngami, Mababe and Linyanti-Chobe sub-basins (After Mosley-Bufford et al., 2012).

CHAPTER IV

METHODS

4.1. Curie point depth analysis (CPD)

4.1.1. Two-dimensional radial power density spectral analysis

The aeromagnetic data (Figure 3) used in this study were acquired in 1996 by the Geological Survey of Botswana at a flight altitude of ~80 meters along N-S lines with line spacing of 250 meters and E-W tie lines with 1.25 kilometers separation. The international geomagnetic reference field was removed from the data. The data were provided in grid cell size of 62.5 meters.

Traditionally, the Curie Point Depth (CPD) is determined using spectral methods [Spector and Grant, 1970; Bhattacharyya and Leu, 1975; Tanaka *et al.*, 1999] and references therein. The method has been used successfully to determine the regional CPD values over large study areas [Hussein *et al.*, 2012]. The major drawback associated with the spectral method is in imaging small scale variations in CPD values [Hussein *et al.*, 2012]. As suggested by Hussein *et al.* [2012], reasonable estimates of depths to the bottom of the magnetic source can be obtained provided that the length and width of the sub-region for which the depth was determined was at least three to four times greater

than the depth of the magnetic source. For example, $1^\circ \times 1^\circ$ cells ($\sim 100 \times 100$ km) are needed in this study to confidently image anomalies to the depth of 25 km. The aeromagnetic anomaly data of the ORZ and surrounding areas were not filtered to remove regional fields or the lowest wavenumbers of the spectrum as suggested by *Ravat et al.* [2007]. Instead, the aeromagnetic anomaly data were reduced to the pole to transform dipolar magnetic anomalies to monopolar anomalies centered over their causative body. In this study, $1^\circ \times 1^\circ$ sub-regions were used. A 25 km overlap in the X and Y directions were used as suggested by *Hussein et al.* [2012] to ensure consistency of results. *Tanaka et al.* [1999] showed that the depth to the base of the magnetic source of a region can be calculated using 2D power-density spectrum analyses approach. The function estimates the depth to the top of the magnetic source by fitting a straight line through the highest wavenumber portions using the equation:

$$Z_t = \ln [\Phi_{AT} (|k|)^{1/2}] \quad 1$$

where, Φ_{AT} is the radial power density spectra of the total magnetic field and k is the wave number [*Okubo et al.*, 1985]. In this study, we used the $0.5\text{-}0.8 \text{ rad km}^{-1}$ range as has been recommended by *Hussein et al.* [2012]. On the other hand, the depth to the centroid is determined by plotting:

$$Z_c = \ln [\Phi_{AT} (|k|)^{1/2}] / |k| \quad 2$$

and then fitting a straight line through the lower wavenumber ranging between 0.02 and 0.3 rad km⁻¹ as similarly suggested by *Hussein et al.* [2012]. To account for the drawbacks associated with selecting where to measure slope of the low wavenumber in the 2D power-density spectrum analyses method, the slope was measured at three different locations and the average value was used. The depth of the base of the magnetic source (Z_b) is then calculated using the equation:

$$Z_b = 2Z_c - Z_t \quad 3$$

where Z_t and Z_c are the top and centroid of the magnetic sources, respectively. Examples of the 2D power-density spectrum analyses for depth to the magnetic sources estimation are shown in Figures 4a and b. The CPD is calculated by using the relationship ($Z_b = 2Z_c - Z_t$). In this case $Z_b = 2 \times 10 \text{ km} - 6.67 \text{ km}$; $Z_b = 13.33 \text{ km}$.

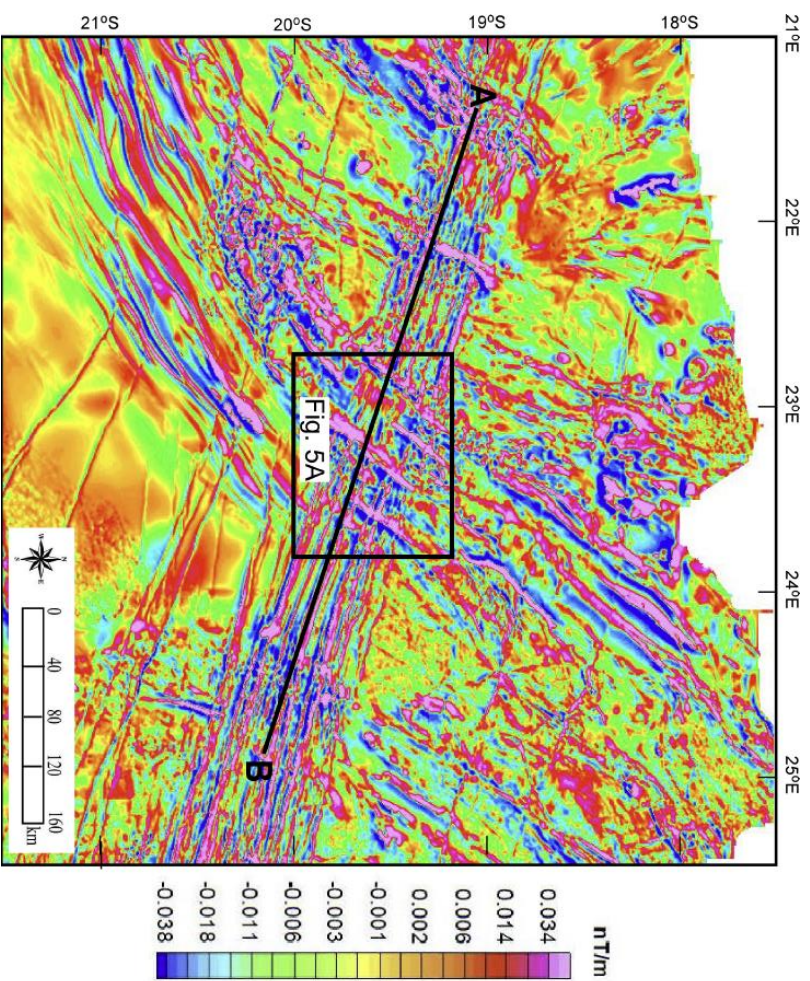


Figure 3. The aeromagnetic map of the Okavango Rift Zone. The NE-trending magnetic anomalies are the result of regional foliation and folding within the Damara-Ghanzi-Chobe belt. The NW-trending magnetic anomalies represent the Okavango Dike Swarm. The profile A-B is the location of the cross-section presented in Figure 5b.

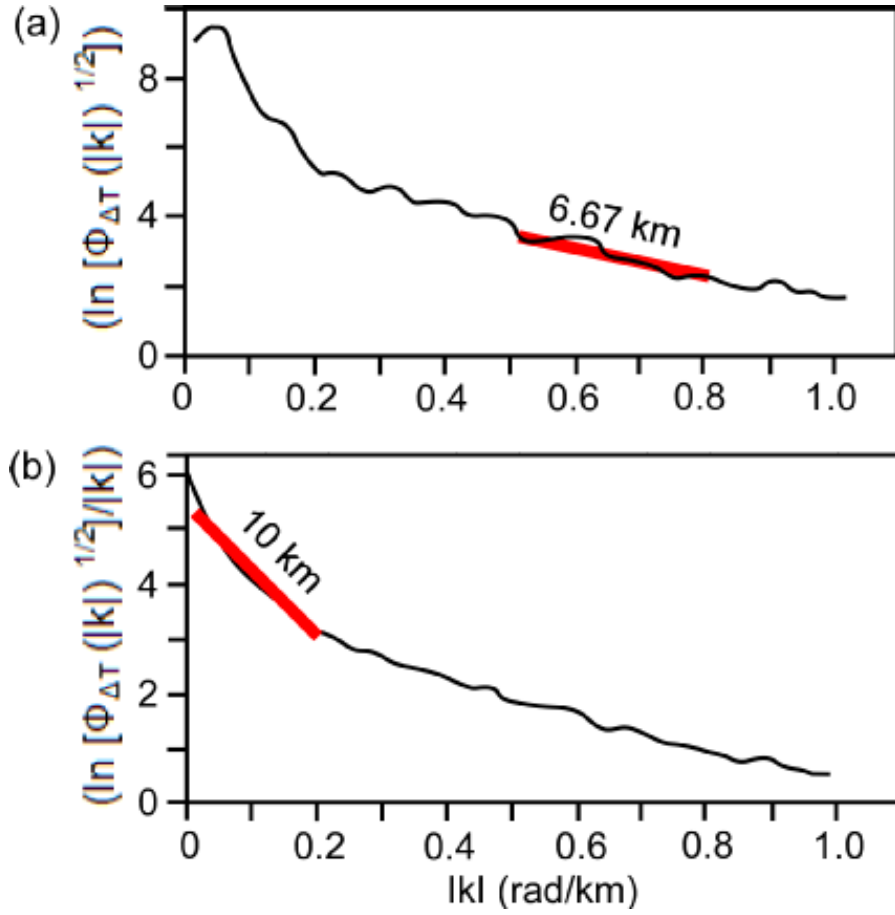


Figure 4. (a) An example of the 2D power-density spectrum analyses used for the computation of the top of the magnetic source (Z_t) values using the relationship $(\ln [\Phi_{\Delta T} (|k|)^{1/2}])$ and the lower wavelength number of 0.5-0.8 rad/km. (b) An example of the 2D power-density spectrum analyses used for the computation of the centroid (Z_c) using the relationship $(\ln [\Phi_{\Delta T} (|k|)^{1/2}/|k|])$ and the high wavenumber of 0.02-0.3 rad/km $\Phi_{\Delta T}$ is the radial power density spectrum of the total magnetic field and K is the wave number.

4.1.2. Three dimensional inversions

To test the validity of our results from the 2D power-density spectrum analyses and to provide a detailed graphic representation of the geometry and extent of magnetization below surface, we inverted the magnetic anomaly for a 3D magnetic susceptibility distribution using the inversion program of *Li and Oldenburg* [1996]. Similar to the 2D power-density spectrum analyses, we used $1^\circ \times 1^\circ$ sub-regions. Additional parameters included maximum mesh depth of 50 km and grid cell size of 900 meters which gradually decreases towards the edges. We used the depth weighting procedure [*Li and Oldenburg*, 1996; *Hussein et al.*, 2012] to circumvent the problem of magnetic bodies possibly occurring near the surface. Other parameters such as weighting of the data, data errors, starting models and mesh size were constantly adjusted so that the magnetic model reflects the geology of the area. Figure A2 shows both the magnetic anomalies and the calculated magnetic anomalies before and after inversion. Figure 5a shows the observed 3D inversion model of a sub-region ($1^\circ \times 1^\circ$) and E-W depth slices (labeled a, b, c, d, and e) illustrating the 3D inversion of the aeromagnetic data used for the calculation of Curie Point Depth.. The CPD is inferred as the depth below the magnetic source. Cross-section of models along profiles perpendicular to the ORZ were merged to illustrate the distribution of magnetic source below the rift, cratons, and the orogenic belt (Figure 5b,) 3D inversion model for cross-section A-B are displayed in the Appendix as Figures A2, A,3 A4, A5, A6, A7, A8, A9, A10, A11 and A12).

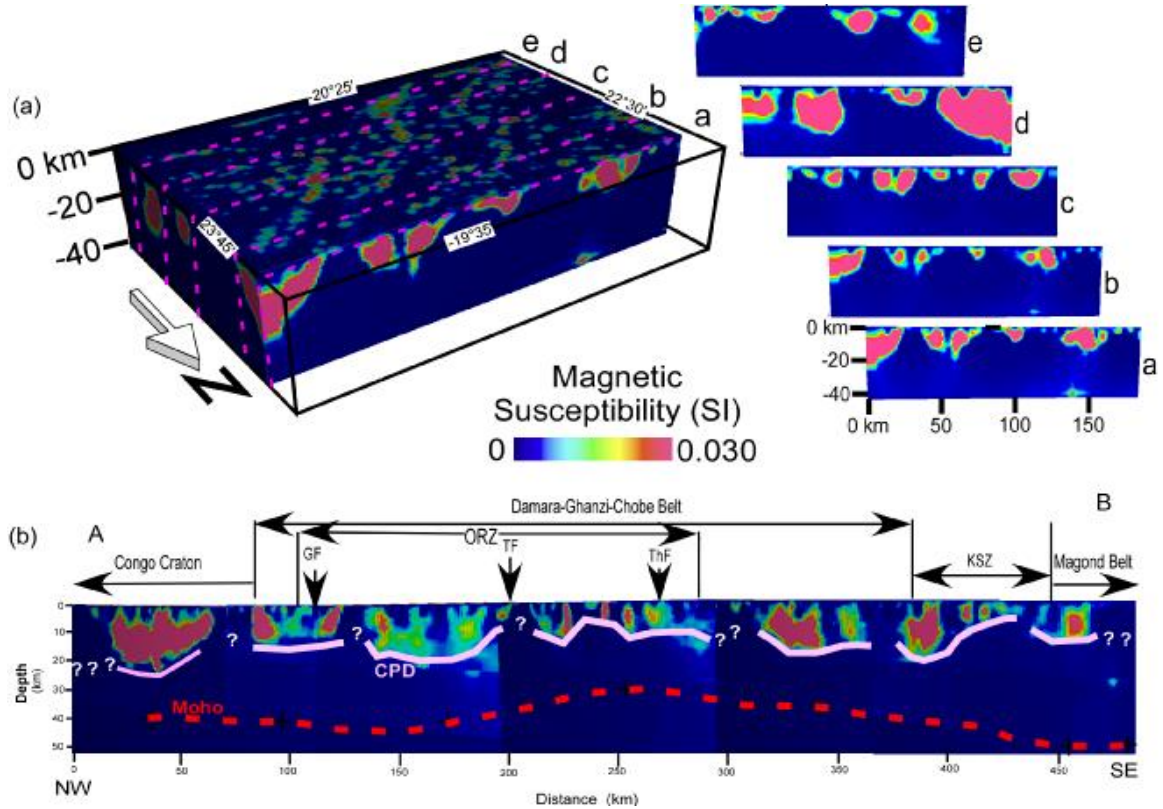


Figure 5. (a) An example of $1^\circ \times 1^\circ$ sub-block with ~40 depth and E-W depth slices (labeled a, b, c, d, and e) illustrating the 3D inversion of the aeromagnetic data used for the calculation of Curie Point Depth. The sub-block is from the southwestern part of the Okavango Rift Zone. (b) 3D inversion cross-section along a NW-SE profile showing the distribution of magnetization beneath the Okavango Rift Zone and surrounding terrains. GF= Gumare Fault. TF= Tsau Fault. ThF= Thamalakane Fault. KSZ= Kalahari Suture Zone. The pink and red lines are the approximate base of magnetization and Moho depth respectively. The blocks used in the cross section are presented in the Appendix as Figures A3, A4, A5, A6, A7, A8, A9, A10, A11 and A12.

4.2. Heat flow estimates from CPD

The 1D Fourier's Law conductive heat flow equation that assumes constant temperature gradient was used to calculate the heat flow values under the ORZ and surrounding cartons and orogenic belts. Fourier's Law is given by:

$$q=k(dT/dz) \quad 4$$

where variables dT/dz , q and k are the temperature gradient, heat flux and the thermal conductivity, respectively. *Tanaka et al.* [1999] showed that the Curie temperature, C , can be defined as:

$$C=(dT/dz)D \quad 5$$

where D is the CDP. If we assume that there are no other heat sources between surface and the CPD, equation 5 can be reduced to:

$$D=kC/q \quad 6$$

The variable k is the thermal conductivity that is directly related to the nature of geologic materials [Lillie, 1999]. The overall pattern of heat flow in the study area is calculated using (Equation 6) assuming average thermal conductivity of ($1.3 \text{ m}^{-1}\text{k}^{-1}$) and Curie temperature of $580 \text{ }^{\circ}\text{C}$. The thermal conductivity was influenced by the presence of granitic basement that dominate most of the study area.

4.3. Crustal thickness (Moho depth)

The 7.5 km cell size grid Bouguer anomaly map of northwestern Botswana (Figure 6) obtained from the Geological Survey of Botswana was used in the crustal thickness estimation. In addition, gravity data collected by various mineral exploration groups, as well as data collected during this study were added to the 7.5 km cell size grid gravity data. The 2D power-density spectrum analyses was used to estimate the crustal thickness beneath the ORZ and surrounding cratons and orogenic belts following the procedure of *Tselentis et al.* [1988].

To evaluate the reliability of our Moho depth estimation, we calculated the crustal thickness of eight blocks centered on the same locations of passive seismic stations used in estimating crustal thickness from previous studies (Table A1) [*Nguuri et al.*, 2001; *Nair et al.*, 2006; *Kgaswane et al.*, 2009]. The 2D radial power spectrum is plotted against the wavenumber and a series of points represented by one or more straight lines in Layer 2 on the graph are used to calculate the crustal thickness (Figure 7). The slope of the points together with the standard error of the best fit were calculated and the corresponding depth and error depth to the appropriate discontinuity for each gridded data [*Tselentis et al.*, 1988].

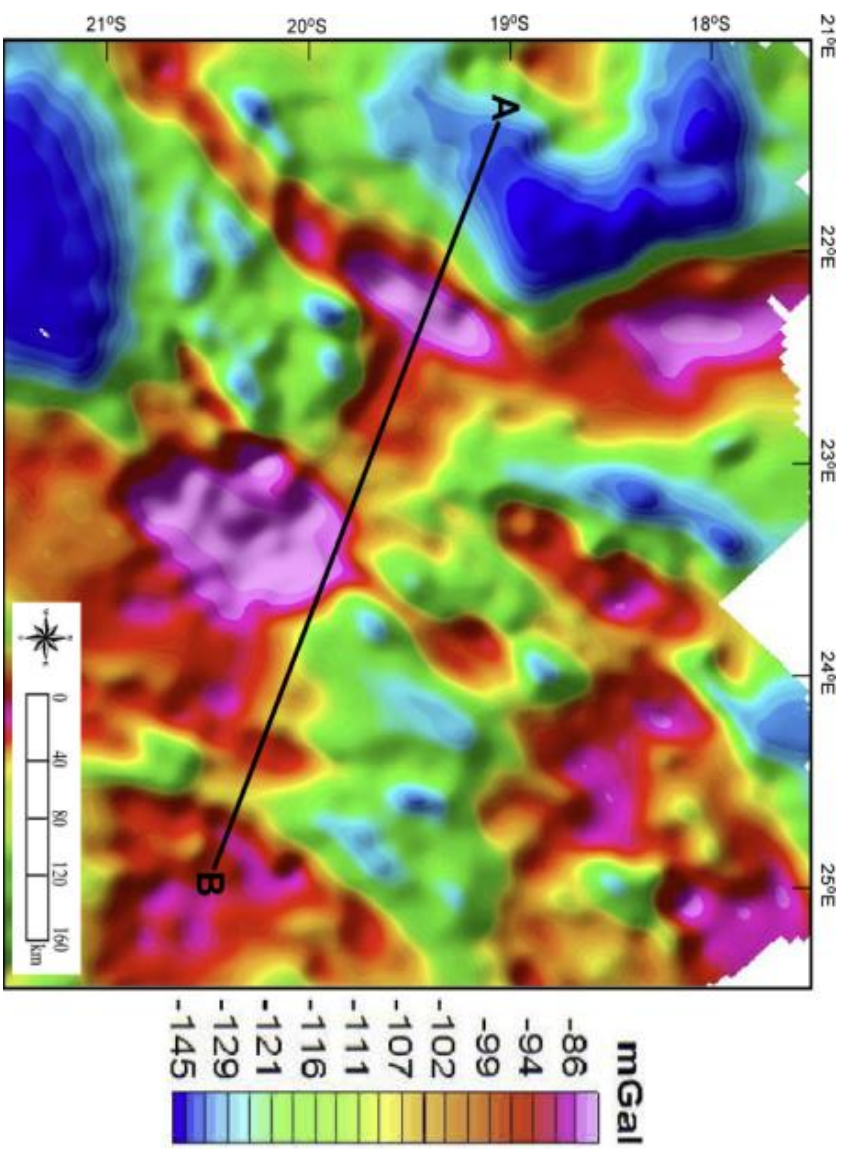


Figure 6. The Bouguer anomaly map used for estimating the crustal thickness in northern Botswana through the 2D power-density spectrum analyses. The profile A-B is the location of the cross-section presented in Figure 10.

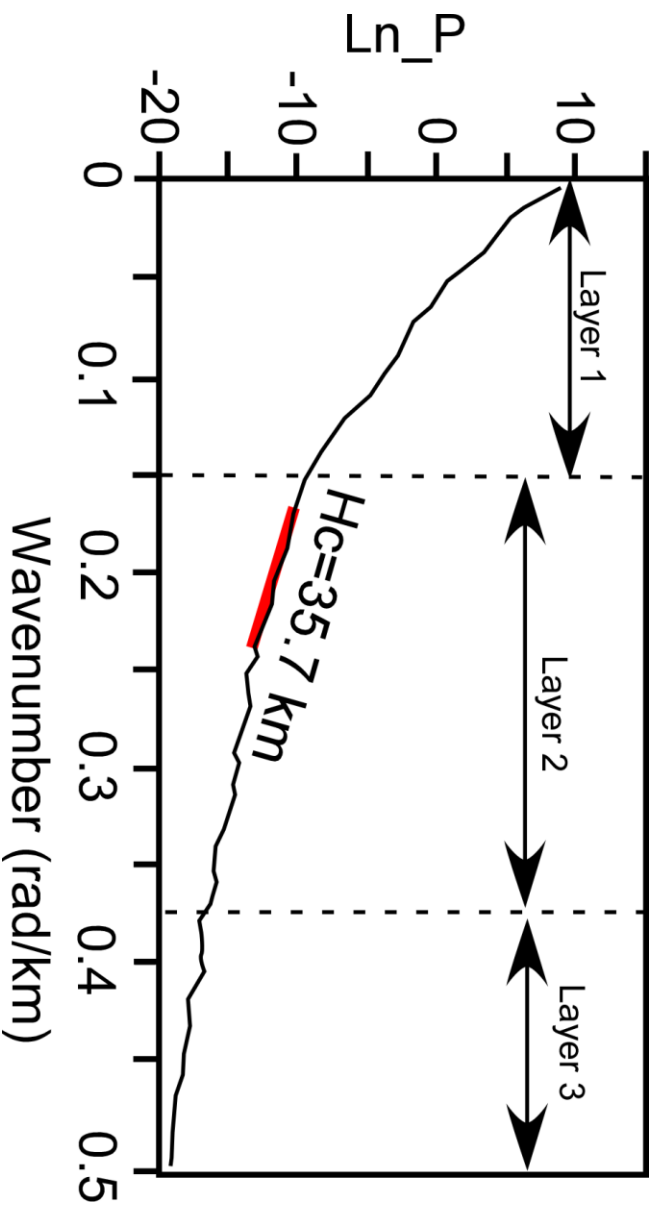


Figure 7. An example of the 2D power-density spectrum analysis curve used for the estimation of the crustal thickness values. The radial power spectrum is plotted against the wavenumber and a series of points which are represented by one or more straight lines in Layer 2 on the graph are used to calculate the crustal thickness.

CHAPTER V

RESULTS

5.1 Curie Point Depth (CPD)

The major trends observed in the CPD are similar in both the 2D power-density spectrum (data not presented) analyses and 3D inversion methods although the values are slightly different. First, for the most part, the deepest CPD values are encountered outside the ORZ and the shallowest CPD values are found within the rift itself (Figures 5b and 8). The CPD values are as shallow as 8 km within ORZ. On the other hand, the CPD values outside the ORZ are as deep as 23 km. Second, the northeastern part of the ORZ is generally characterized by shallower CPD values compared to its southwestern part. In the northeast where the rift basin is more developed and underlain by the Linyanti-Chobe sub-basin, the CPD values range between ~9 km and ~17 km. The CPD estimates in the southwestern part of the rift range between ~12 and ~17 km within Ngami sub-basin (Figure A2) and these values decrease progressively to the northeast reaching 7 km within the Mababe sub-basin (Figure 8). It is worth mentioning here that, in the northeast, the rift narrows to ~60 km width defined by closely-spaced NE-trending normal faults. A hot spring with 45°C measured temperature has been reported in the northeastern part of the ORZ [Niles, *personal comm.* 2013]. Third, the deepest CPD values are found in the

southwestern part of the ORZ where the rift is wider reaching 150 km (Figure 8). These values are nearly as deep as those observed in the surrounding cratons and orogenic belts. This is also close to where the rift terminates further to the southwest.

In general, regardless of the northeast shallowing of the CPD values, there seems to be a cluster of shallow CPD values in the southeastern margin of the ORZ, especially close to the Tsau and Thamalakane faults, where most subsidence and high concentration of faults occur (Figure 8) [*Modisi et al.*, 2000; *Kinabo et al.*, 2007; 2008; *Shemang and Molwalefhe*, 2009]. This zone is defined by CPD values ranging between 7 km and 14 km. The region of shallow CPD values coincides with the Linyanti-Chobe, Mababe and Ngami sub-basins. Further southeast, on the footwall of the ORZ, the CPD values increase from 17 km to 20 km (Figure 8).

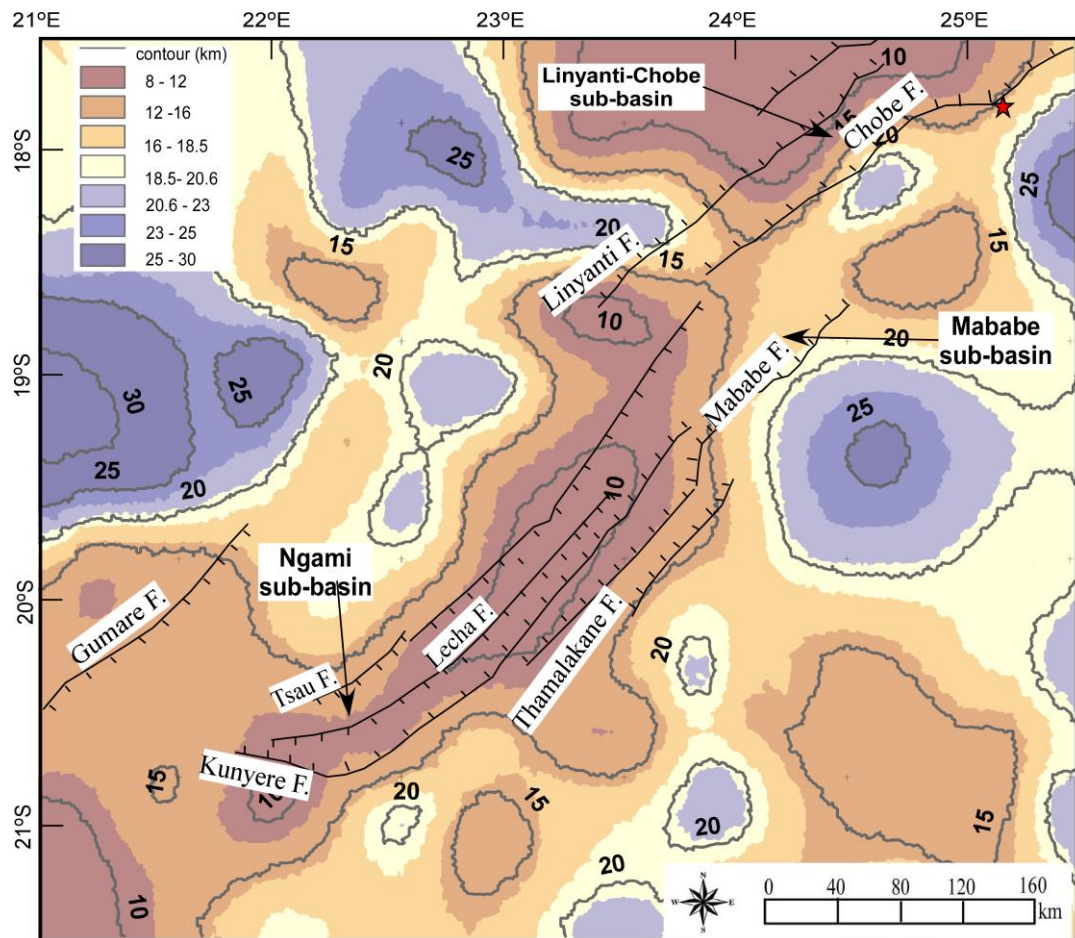


Figure 8: Curie Point Depth values in kilometers obtained from the 3D inversion method for the Okavango Rift Zone (ORZ) and surrounding regions. The red star is the hot spring with temperature of 43 °C. The hatched lines are normal faults.

5.2. Heat Flow

The ORZ and the immediate surroundings are characterized by heat flow values ranging between ~ 38 and 83 mWm^{-2} (Figure 9). Similar to the CPD values, the heat flow values increase from southwest where the rift is wider to northeast where it is narrower. The highest heat flow values seem to concentrate on the southeastern margin of the ORZ and these values are consistent with in situ borehole measurement of heat flow by *Ballard et al.* [1987]. The highest heat flow values are estimated in the vicinity of the Mababe sub-basin between the Tsau and Thamalakane faults (Figure 9). In this sub-basin these values are as high as 83 mWm^{-2} . Similarly, the Linyanti-Chobe sub-basin shows elevated heat flow values reaching 83 mWm^{-2} close to the location of a hot spring (Figure 9). The Ngami sub-basin is characterized by heat flow values ranging between ~ 53 and $\sim 47 \text{ mWm}^{-2}$. The heat flow values progressively decrease to the southeast outside the ORZ reaching 38 mWm^{-2} (Figure 9).

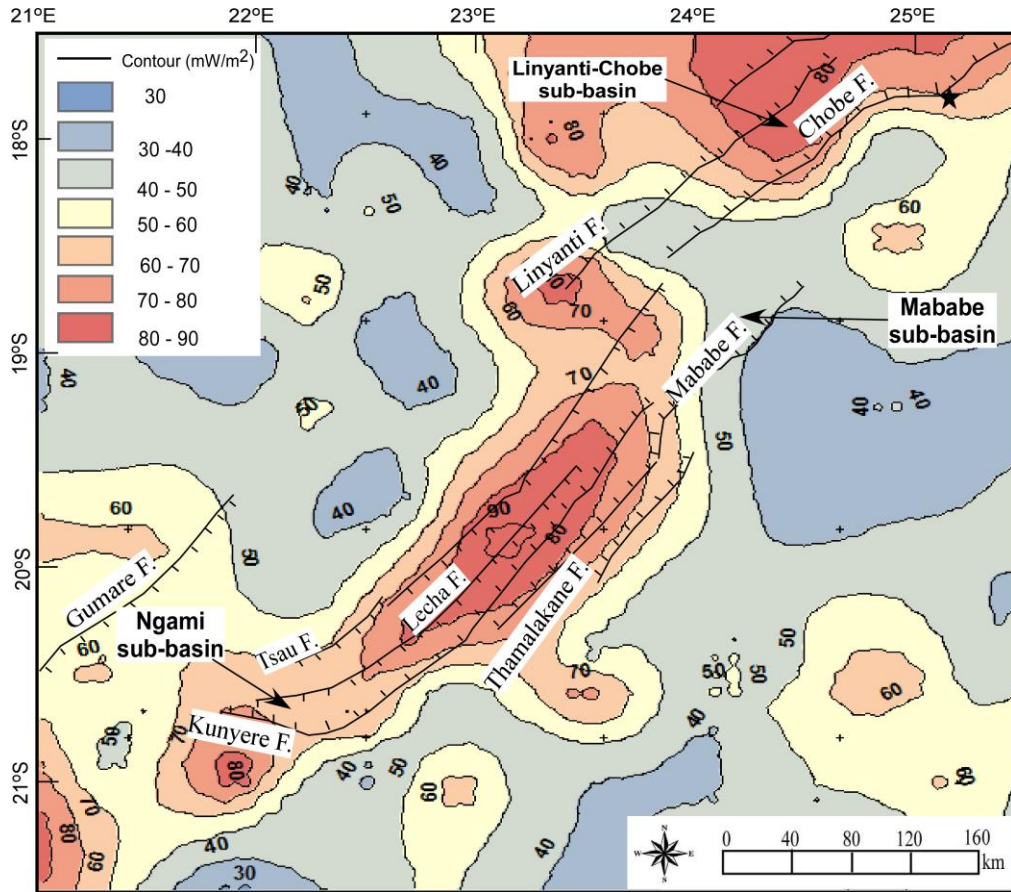


Figure 9. Map of heat flow values in mWm^2 calculated using Curie point depth from 3D inversion results. The red circles are heat flow values from borehole measurement by *Ballard et al.* [1987]. The black star is the hot spring with temperature of 43 °C. The hatched lines are normal faults.

5.3. Crustal thickness (Moho depth)

Figure 5b shows the Moho results along a NW-SE profile across the ORZ and different terrains. The Moho beneath the Congo craton is estimated to be approximately 40 km. To the southeast, the Moho thickens beneath the boundary with the Damara-Ghanzi-Chobe orogenic belt is approximately 45 ± 3 km. The rift is defined by much shallower Moho depths of $\sim 27\pm3$ km and 30 ± 3 km beneath the Ngami sub-basin. Towards the Kalahari Suture Zone there is a gradual increase in depths to 40 ± 3 km. The boundary between the Magondi belt and the Kalahari Suture Zone is defined by a thick Moho approximately 53 ± 3 km. The results beneath the boundary of the Kalahari Suture Zone and the Magondi orogenic belt is in good agreement with the results obtain in the vicinity of Okwa terrane using P and S seismic wave [Nguuri *et al.*, 2001; James *et al.*, 2003]. The result for the average crustal thickness in the northern part of Botswana is presented in the Appendix (Figure A13).

Table 1. Crustal thickness estimation from gravity compared to data from passive seismic stations in eastern Botswana from the Kaapvaal project.

Seismic tation	Latitude deg,	Longitude deg,	Gravity method (km)	<i>Nguuri et al., 2001</i> (km)	<i>Nair et al., 2006</i> (km)	<i>Kgaswane et al., 2009</i> (km)
sa63	-23.658	26.082	44.66± 3	50-47	44.4±1.12	N/A
sa64	-22.969	26.202	45.3±3	44-41	41.2 ± 0.58	40.5
sa65	-22.818	27.222	48.5±3	50-47	43.1±0.07	40.5
sa66	-21.9	26.373	45.4±3	50 - 47	46.9 ±0.16	48
sa67	-21.886	27.274	45.9±3	47 - 44	N/A	45.5
sa68	-21.95	28.188	45±3	50 - 47	50.3 ± 1.19	45.5
sa70	-21.088	26.335	54.3±3	53 - 56	51.6 ±0.23	50.5
sa 71	-20.926	27.141	44.3±3	47 - 44	43.6 ± 0.85	43.0

CHAPTER VI

DISCUSSIONS

6.1. Thermal structure beneath the ORZ and surrounding cratons and orogenic belts

The Curie point is the temperature at which crustal materials lose their ability to be permanently magnetized. The depth at which this temperature is reached is mainly controlled by the geothermal gradient and thermal properties of rocks. These two factors play an important role in controlling the heat flow of a given area [Araniz-Rodrigues and Orihuela, 2013]. Therefore, variations in the CPD values can be correlated with the tectonic processes, especially thermal processes driving rift initiation. Araniz-Rodrigues and Orihuela [2013] classified CPD values into two groups based on their position relative to the Moho depth: (1) CPD values shallower than the Moho are usually associated with areas with high heat flow resulting from crustal thinning; and (2) CPD values deeper than the Moho are typical of tectonically and isostatically stable areas with low heat flow.

The CPD values of the ORZ and the surrounding regions obtained show shallower values within the rift and deeper values outside the rift beneath the cratons and orogenic belts (Figures 5 and 8). *Deen et al.* [2006] have shown that most of northwestern Botswana and Namibia are underlain by high heat flow values ($42 - 60 \text{ mWm}^{-2}$) and that this region is bounded in the northwest and southeast by NW-trending belts of low heat flow values ($> 40 \text{ mWm}^{-2}$) corresponding to the Congo and Kalahari cratons.

The CPD values within the Linyanti-Chobe, Mababe and Ngami sub-basins are shallowest reaching ~ 9 km within the Linyanti-Chobe sub-basin in the northeast (Figure 8). Previous studies have suggested that this is the more developed part of the ORZ [*Kinabo et al.*, 2007; 2008]. The shallow CPD values in the northeastern part of the ORZ coincide with the location of a hot spring with a surface temperature of 43°C [*Niles, personal comm.*]. Correlating our results with the geological map of *Singletary et al.* [2003], the CPD data suggests that the deep magnetic anomalies are mainly located under Precambrian lithologies.

The heat flow values from the magnetic analysis (Figure 9) confirm elevated heat flow beneath the ORZ compared to those beneath the cratons and surrounding orogenic belts. Additionally, these values are similar to those obtained from in situ borehole measurements [*Ballard et al.*, 1987]. For example, near the Mababe sub-basin, our estimated heat flow of 47 mWm^{-2} is comparable to $\sim 56 \text{ mWm}^{-2}$ value obtained from borehole data by *Ballard et al.* [1987]. Also, the heat flow value of the $\sim 53 \text{ mWm}^{-2}$

estimated in the Ngami sub-basin is comparable to the 60 m W/m^{-2} value measured in boreholes by *Ballard et al.* [1987]. These values are also similar to regional heat flow values from inversion of passive seismic data [*Deen et al.*, 2006].

Similar elevated heat flows are also reported in parts of the Western Branch of the EARS in the Albertine rift and have been associated with thinned lithosphere coupled with ascending melt enhanced by a network of faults [*Wolbern et al.*, 2012]. Also shallow CPD values ranging between ~ 5.2 and ~ 8.3 km from the Eastern Branch in the southern Kenya rift have been interpreted as indicating high heat flow associated with the presence of magma body at depth [*Githiri et al.*, 2012]. Similarly, CPD estimates from the Death Valley and surrounding areas in the United States showed that the shallowest CPD values (<15 km) occur over known geothermal fields, hot springs region and a seismically-imaged magma body, whereas deeper values (>15 km) occur beneath Precambrian lithologies [*Hussein et al.*, 2013].

Preliminary results from Teleseismic P-wave travel-time residuals show a delay of 1 s at stations in the Okavango rift relative to the Limpopo belt originating from an earthquake with an epicenter located in the Indian Ocean [*Gao et al.*, 2013]. Moreover, MT results across the Barotse Basin in Zambia northeast of the Chobe-Linyanti sub-basins suggests that the continental lithosphere is characterized by an anomalous low resistivity of $1\text{-}10 \text{ } \Omega\text{m}$, significantly different from the normal resistivity of $1000 \text{ } \Omega\text{m}$ that characterizes typical continental lithosphere [*Evans, personal comm.*]. Similar conductive

zones in the middle to lower crust have been imaged using MT below the Main Ethiopian Rift and interpreted as zones of partial melts [Whaler and Hautot, 2006]. We note that similar mid-shallow crustal conductors were observed in the MT results of Khoza *et al.* [2013] within the central zone of the Damara-Ghanzi-Chobe belt. In fact, the crustal conductors are well known features in MT images of this orogenic belt [Ritter *et al.*, 2003; Khoza *et al.*, 2013 and reference there in]. The source of these conductors is debatable but has been attributed to graphite bearing marbles [Ritter *et al.*, 2003] or massive sulfide mineralization [Khoza *et al.*, 2013].

6.2. Moho structure and thermal perturbations

To determine how good our Moho depth estimates are, we first of all determined Moho depths at locations outside our study area where Moho depths have been estimated from three different seismic studies [Table A1]. Table A1 shows that our Moho depth estimates are comparable to depths obtained from the seismic studies. Thus we are confident that our depth estimates from the ORZ are reasonable. The Moho estimates from spectral analysis suggest that the crust below the ORZ is thinner than it is under the adjacent Precambrian cratons and orogenic belts. Interestingly, beneath the ORZ in the vicinity of the Ngami sub-basin, we estimated the crustal thickness to be 30 km (Figure 5b). This is consistent with the Moho depth estimates from several studies along other segments of the EARS indicative of a thinned (20 km) crust below the rift axis compared

to ~40 – 50 km thick crust below undisturbed cratons and orogenic belts [*Mickus et al.*, 2007].

During horizontal extension, lithospheric stretching results in vertical thinning of the crust causing increase in the geothermal gradient within the zone of thinning [*McKenzie*, 1978]. The upward movement of the asthenosphere results in the increase in heat flow below rifts. This process results in a net weakening of the lithosphere, whose integrated strength is highly sensitive to temperature [*Kearey et al.*, 2009]. *Grovers and Wortel* [1993] suggested that heat-producing radioactive elements migrate to the crust and significantly increase the geothermal gradient during thinning. *Omenda* [2010] suggested that lithospheric necking processes elevate the geothermal gradient beneath the EARS. Our results show that the ORZ is associated with high heat flow and elevated crustal geotherms within, at least, the 60 km narrow zone of the area bounded by the Tsau and Thamalakane border faults (Figure 5b). Where shallow CPD values are encountered in the southeastern margin of the ORZ, the crust is significantly thinned and this is manifested in the development of three sub-basins of the ORZ. This is in sharp contrast to the northwestern side of the rift where the Gumare fault (Figure 5b) is acting only as a hinge line of a SE-dipping half graben constituting the southwestern part of the ORZ [*Kinabo et al.*, 2007; 2008; *Mosley-Bufford et al.*, 2012]. The southeastern edge of the rift is also defined by strong NE-trending basement regional fabric, mainly tight folds and faults [*Modisi et al.*, 2000; *Kinabo et al.*, 2007; 2008; *Mosley-Bufford et al.*, 2012].

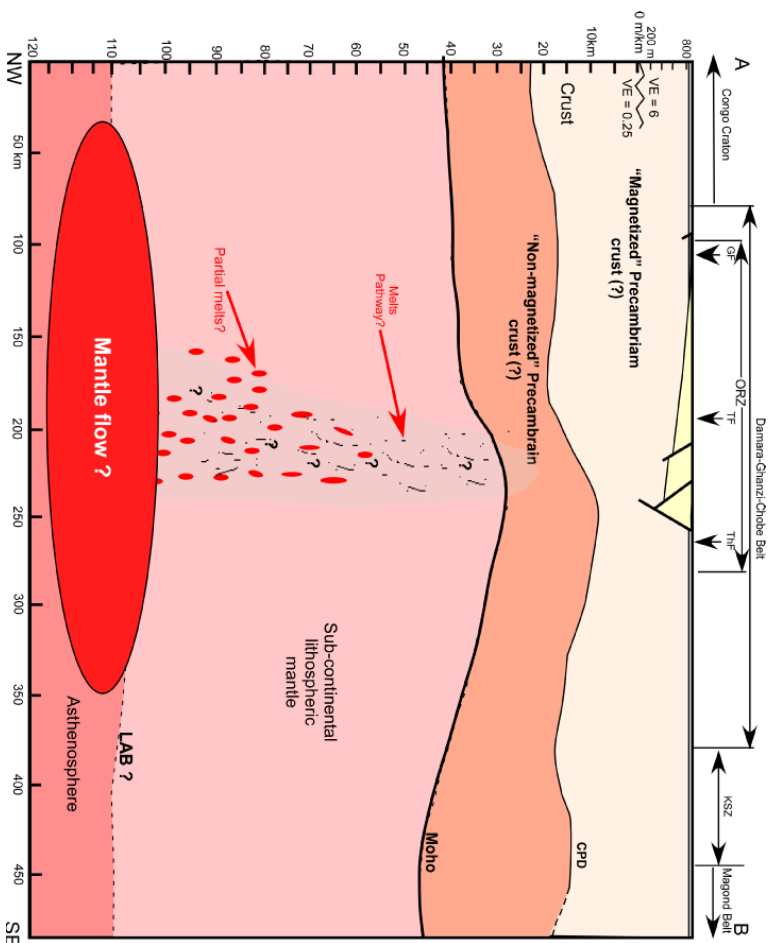


Figure 10. A schematic NW-SE cross-section along profile A-B shown in Figure 3 and 6 illustrating the lithosphere and thermal structure of the Okavango Rift Zone. The Shallow Curie Point Depth (CPD), Moho, and elevated lithosphere/asthenosphere boundary as found under the rift.

6.3. Pre-existing structures and thermal perturbation

Most of the normal faults of the ORZ are parallel to the NE-trending basement fabric of the Damara-Ghanzi-Chobe orogenic belt. Previous studies by *Modisi et al.* [2000] and *Kinabo et al.* [2007; 2008] have highlighted the important role that pre-existing structures play in localizing strain in the ORZ. The elevated geothermal gradient and the shallow CPD values occur within the pronounced basement fabric in the southeastern side of the rift. We suggest that the presence of strong basement fabric, especially in the southeastern side of the ORZ might have facilitated upward migration of hot fluid, hence locally increased the geothermal gradient in this region as observed by the CPD values and heat flow estimates.

6.4. Source of thermal anomalies below the ORZ

Assuming that the CPD values in Figure 8 are independent of the magnetic properties of different lithological units, we propose that the shallower CPD values beneath the ORZ are the result of thermal perturbations. This finding is in contrast with recent MT results suggesting that the ORZ lacks a typical rift signature of a thinned lithosphere coupled with the presence of a thermal anomaly [*Khoza et al.*, 2013]. *Khoza et al.* [2013] argued that if rifting is indeed taking place in the ORZ, then it must be initiated through uppermost crustal processes without the involvement of asthenospheric

processes. Differently, our findings point to a major role of asthenospheric processes in the initiation of the ORZ. Our results are further supported by preliminary Teleseismic P-wave travel-time residuals show a delay of 1 s at stations in the Okavango rift relative to the Limpopo belt the ORZ indicative of a thin lithosphere and possibly the presence of a shallower asthenospheric material [*Gao et al.*, 2013].

The presence of thermal perturbation under the rift system could be attributed to the presence of a mantle plume, small-scale convection in the asthenosphere driven by the adjacent cold edge of the Congo and Kalahari Cratons, or channelized mantle flow. The presence of a mantle plume under the ORZ is unlikely as preliminary seismic results do not show a perturbed mantle transition zone [*Yu et al.*, 2013]. Also, the presence of such a plume will lead to outpouring of large amount of volcanism to the surface, hence the development of magmatic rift system. Surface geology observations show that the ORZ is amagmatic and no volcanism is observed within the rift system.

The development of the ORZ within the Damara-Ghanzi-Chobe orogenic belt between the Congo and Kalahari cratons makes it tempting to consider the source of the thermal anomaly as due to edge-driven convection. This proposition remains to be tested with future geophysical studies. However, the current shear-wave splitting results does not support this model. These results show that majority of the shear-waver splitting measurement indicate faster splitting time in a NE-direction, parallel to the strike of the ORZ [*Gao et al.*, 2013]. The presence of small-scale convection under rifts usually

results in shear wave splitting pattern in which the fast splitting time is perpendicular to the strike of the rift. This is best exemplified by the shear wave splitting measurements from the Baikal rift zone [*Gao et al.*, 1994]

We hypothesize that the source of the thermal anomaly beneath the ORZ results from a melt/fluid infiltration front concentrated along vertical oriented intersections of preexisting crustal fault systems. These fluids could be derived from channelized mantle flow, possibly directed in a NE-SW direction due to a thinner lithosphere under the Damara-Ghanzi-Chobe orogenic belt surrounded by the thicker lithosphere of the Congo and Kalahari cratons. This mantle flow could have originated from the African mantle super plume. This might be explained by the origin of the NE-trending fast splitting time in the shear wave splitting measurements under the ORZ. We downplay the contribution of the NE-trending regional fabric of the orogenic belt to the faster splitting time direction because if the source of the shear wave splitting measurements is the shallower upper crust anisotropy then the faster splitting time direction would have been in both NE and NW direction. This is because the extent of the Okavango Dike swarm present a strong upper crust NW-trending anisotropy, hence resulting in the faster splitting time in that direction.

Our findings are summarized in a schematic cross-section (Figure 10) along a NW-SE idealized transect illustrating the lithosphere and thermal structure and processes responsible for rift initiation beneath the Okavango Rift Zone. We propose a significantly

elevated CPD values beneath the ORZ with an asymmetrical structure focused on the southeastern side of the rift. The shallowest CPD values reach 10 km below the central part under the rift accompanied by a thinned continental crust allowing for the Moho to rise to a shallow level of ~30 km. Our model suggests a localized elevated geotherms abetted by pre-existing lithospheric structures that provide a conduit for asthenospheric melts ascending in the sub-continental lithospheric mantle through a dense network of crystalized veins similar to the observation made under the Tanzania craton and the Albertine rift [Jekovlev *et al.*, 2013].

CHAPTER VII

CONCLUSION

2D power-density spectrum analyses and 3D inversion of magnetic data show that the Curie isotherms under the nascent ORZ are shallower than the surrounding cratons and orogenic belts. The distribution of the CPD values under the ORZ ranges from ~8 km in the northeastern part of the rift to ~16 km in the southwest where the rift terminates. The shallow CPD values suggest the existence of a thermal anomaly under the ORZ. This thermal anomaly is associated with an elevated Moho as indicated by our estimation of a thinner continental crust (~27 and ~30 km) under the rift compare to > 40 km underneath the surrounding cratons. The thermal perturbation under the ORZ is supported by preliminary passive seismic results suggesting low P-wave velocity anomaly beneath the rift.

The shallow CPD values, high heat flow values and thin crust within a zone of ~60 km along the southeastern boundary of the ORZ coincide with a strong NE-trending basement fabric, possibly acting as conduits for upward migration of hot fluids. The high heat flow and thinned crust beneath ORZ are possibly due to thermal perturbation in the

in the lithosphere beneath the rift. The possible cause of thermal perturbations under the ORZ might be due to ascending melt infiltration fronts derived from a possible NE-trending mantle flow, possibly extending from the African mantle plume and directed by the thinner lithosphere under the Damara-Ghanzi-Chobe orogenic belt between the Congo and Kalahari Craton.

CHAPTER VIII

FUTURE WORK

This research on ORZ has enhanced our understanding of the thermal structure of the incipient rifts in amagmatic settings and the relationship between the asthenospheric processes and the role that heat plays in strain localization during the initial stages of rifting. However, currently there is no data on estimates of strain rates. Geodetic studies are needed to understand to provide this critical information. Furthermore, lithospheric scale studies such as Magnetotellurics and seismic tomography similar to the study by *Jekovlev et al.* [2009] are needed to better constrain the processes responsible for the proposed thermal anomaly beneath ORZ. The study will help in mapping the conduits and possible partial melts migrating upwards into the upper crust resulting in the disturbed geothermal gradient.

REFERENCES

- Aboud, E., A. Salem and M. Mekkawi (2011), Curie depth map for Sinai Peninsula, Egypt deduced from the analysis of magnetic data, *Tectonophysics*, 506, 46-54.
- Araniz-Rodriques, M. S., and N. Orihuela (2013), Curie point depth in Venezuela and the Eastern Caribbean, *Tectonophysics*, 590, 38-51.
- Ballard, S., H. N. Pollack, and N. J. Skinner (1987), Terrestrial heat flow in Botswana and Namibia, *Journal of Geophysical Research*, 92, 6291-6300.
- Bastow, D. I., A. A. Nyblade, G. W. Sturt, T. O. Rooney and M. H. Benoit (2008), Upper mantle seismic structure beneath the Ethiopian hot spot: Rifting at the edge of the African low-velocity anomaly, *Geochemistry, Geophysics, Geosystems*, 9, 1-25.
- Begg, G. C., W. L. Griffin, L. M. Natapov, S. Y. O'Reilly, S. P. Grand, C. J. O'Neill J. M. A. Hronsky, D. Y. Poudjom, C. J. Swain, T. Deen and P. Bowden (2009), The lithospheric architecture of Africa: seismic tomography, mantle petrology, and tectonic evolution, *Geosphere*, 5, 23–50 doi:10.1130/GES00179.1.
- Bhattacharyya, B. K., (1964), Magnetic anomalies due to prism-shaped bodies with arbitrary polarization, *Geophysics*, 29, 517-553.

- Bhattacharyya, B. K., and L. K. Leu (1975), Analysis of magnetic anomalies over Yellowstone National Park: mapping of Curie point isothermal surface for geothermal reconnaissance, *Journal of Geophysical Research*, 80, 4461-4465.
- Buck, W. R. (2006), The role of magma in the development of Afro-Arabian Rift System, *Journal of the Geological Society*, London, 259, 43-54.
- Chorowics, J. (2005), The East Africa rift system, *Journal of African Earth Sciences*, 43, 379-410.
- Craig, T. J., J. A. Jackson, K. Priestley and D. McKenzie (2011), Earthquake distribution pattern in Africa: their relationship to variation in lithospheric and geologic structure, and their rheological implications, *Geophysical Journal International*, 185, 403-434.
- Deen, T. J., W. L. Griffin, G. Begg, S. Y. O'Reilly, L. M. Natapov, and J. Hronsky (2006), Thermal and compositional structure of the subcontinental lithospheric mantle: Derivation from shear wave seismic tomography, *Geochemistry Geophysics Geosystems*, 7. doi:10.1029/2005GC001120.
- Dolmaz, M. N., T. O. Usta, M. Z. Hisarli and N. Orbay (2005), Curie point depth variations to infer thermal structure of the crust at the African-Eurasian convergence zone: SW Turkey, *Earth Planets and Space*, 57, 373-383.
- Ebinger, C. (2005), Continental break-up: The East African perspective, *Astronomy and Geophysics*, 46, 2.16-12.21.

- Ebinger, C. J. and M. Casey (2001), Continental break-up in magmatic provinces: An Ethiopian Example, *Geology*, 29, 527-530.
- Feucht, D. W., A. F. Sheeha and P. Bedrosian (2013), Deep electrical conductivity structure of the Rio Grande Rift in Colorado and New Mexico: Early results from a two-year magnetotelluric study, *2013 American Geophysical Union Fall Meeting*.
- Gao, S. S., K.H. Liu, C.A. Reed, Y. Yu, B. Massinque, H. Mdala, M. Moidaki, D. Mutamin, E. A. Atekwana, S. Ingate and M.A. Ruesch (2013), SAFARI -Seismic Arrays for African Rift Initiation, *EOS*, 94, 213-214.
- Gao, S. S., P. M. D. H. Liu, P. D. Slack, Y. A. Zorin, V. V. Mordvinova, V. M. Kozhevnikov, and R. P. Meyer (1994), Seismic anisotropy and mantle flow beneath the Baikal rift zone, *Nature*, 371, 149-151.
- Githiri, J. G., J. P. Patel, J.O. Barongo and P.K. Karanja (2012), Spectral analysis of ground magnetic data in Magadi area, Southern Kenya Rift, *Tanzania Journal of Science*, 38, 1-14.
- Grovers, R. and M. J. R. Wortel (1993), Initiation of asymmetric extension in continental lithosphere, *Tectonophysics*, 223, 75-96.

- Hammond, J. O. S., J. M. Kendall, G. W. Stuart, C. J. Ebinger, I. D. Bastow, D. Keir, A. Ayele, M. Belachew, B. Goitom, G. Ogubazghi, and T. J. Wright (2013), Mantle upwelling and initiation of rift segmentation beneath the Afar Depression, *Geology*, 41, 635-638.
- Hussein, M., K. Mickus and F. L. Serpa (2012), Curie point depth estimates from aeromagnetic data from Death Valley and surrounding regions, California, *Pure and Applied Geophysics*, 170, 617-632.
- Jakovlev, A., G. Rümper, M. Lindenfeld, I. Koulakov, A. Schumann and N. Ochmann (2011), Crustal Seismic Velocities of the Rwenzori Region, East African Rift, from Local Travel-Time Tomography: Evidence for Low-Velocity Anomalies beneath the Mountain Range, *Bulletin of the Seismological Society of America*, 101, 848-858.
- James, D. E., F. Niu, J. Rokosky (2003), Crustal structure of the Kaapvaal craton and its significance for early crustal evolution, *Lithos*, 71, 413-429.
- Kampunzu, A.B., P. Akanyang, R.B.M. Mapeo, B.N. Modie and M. Wendorff (1998), Geochemistry and tectonic significance of the Meso-Proterozoic Kgwebe metavolcanic rocks in northwest Botswana: implications for the evolution of the Kibaran Namaqua-Natal belt, *Geological Magazine*, 135, 669-683.
- Kearey, P., K. A. Klepeis and F. J. Vine (2009), Global tectonics, *John Willey & Sons*.

- Kendall, J. M., G. W. Stuart, C. J. Ebinger, I. D. Bastow, and D. Keir (2005), Magma assisted rifting in Ethiopia, *Nature*, 433, 146-148.
- Keranen, K. M., S. L. Klemperer, J. Julia, J. F. Lawrence and A. A. Nyblade (2009), Low lower crustal velocity across Ethiopia: Is the Main Ethiopian Rift a narrow rift in a hot craton? *Geochemistry, Geophysics, Geosystems*, 10, Q0AB01 doi: 10.1029/2008GC002293.
- Kgaswane, E. M., A. A. Nyblade, J. Julia, P. H. G. M. Dicks, R. J. Durrheim and M. E. Pasyanos (2009), Shear wave velocity structure of the lower crust in southern Africa: Evidence from compositional heterogeneity within Archean and Proterozoic terrain, *Journal of Geophysical Research: Solid Earth* 114, 1978–2012, doi: 10.1029/2008JB006217.
- Khoza, D., A.G. Jones, M.R. Muller, R.L. Evans, S.J. Webb, M. Miensoopust, and the SAMTEX team (2013), Tectonic model of the Limpopo belt: Constraints from magnetotelluric data, *Precambrian Research*, 226, 143-156.
- Kinabo, B. D., E. A. Atekwana, J. P. Hogan, M. P. Modisi, D. D. Wheaton and A. B. Kampunzu (2007), Early structural development of the Okavango rift zone, NW Botswana, *Journal of African Earth Sciences*, 48, 125-136.
- Kinabo, B. D., J. P. Hogan, E. A. Atekwana, M. G. Abdelsalam, and M. P. Modisi (2008), Fault growth and propagation during incipient continental rifting: insights from a combined aeromagnetic and Shuttle Topography Mission

- digital elevation model investigation of the Okavango Rift Zone, northwest Botswana, *Tectonics*, 27, 1-16.
- Levander, A. and M. S. Miller (2012), Evolutionary aspect of lithospheric discontinuity structure in the western USA, *Geochemistry, Geophysics, Geosystems*, 13, QOK07, doi.10.1029 /2012GC00056.
- Li, Y. and D. W. Oldenburg (1996), 3-D Inversion of magnetic data, *Geophysics*, 61, 394-408.
- Lillie, R. J. (1999), Whole Earth Geophysics-An Introductory Textbook for Geologists and Geophysicists, *Prentice Hall*, Upper Saddle River, New Jersey.
- Maguire, P. K. H, G. R. Keller, S. L. Klemperer, G. D. Mackenzie, K. Keranen, S. Harder, B. O'Reilly, H. Thybo, L. Asfaw, M. A. Khan, and M. Amha (2006), Crustal structure of the northern Main Ethiopian Rift from the EAGLE controlled-source survey; a snapshot of incipient lithospheric break-up, *Geological Society of London Special Publications*, 259, 269–291.
- McKenzie, D. (1978), Some remarks on the development of sedimentary basins, *Earth and Planet Science Letters*, 40, 25-32.
- Mackenzie, G. D., H. Thybo, and P. K. H. Maguire (2005), Crustal velocity structure across the Main Ethiopian Rift: results from two-dimensional wide-angle seismic modeling, *Geophysical Journal International*, 162, 994–1006.

- Mickus, K., K. Tadesse, G. Keller, and B. Oluma (2007), Gravity analysis of the Main Ethiopian Rift, *Journal of African Earth Sciences*, 48, 59-69.
- Miensopust, M. P., A. G. Jones, M. R. Muller, X. Garcia and R. L. Evans (2011), Lithospheric structures and Precambrian terrane boundaries in northeastern Botswana revealed through magnetotelluric profiling as part of the Southern African Magnetotelluric Experiment, *Journal of Geophysical Research*, 115, 1-21.
- Modisi, M. P., E.A. Atekwana, A.B. Kampunzu, and T.H. Ngwisanyi (2000), Rift kinematics during the incipient stages of continental extension: evidence from the nascent Okavango rift basin, northwest Botswana, *Geology*, 102, 363-376.
- Moore, A. E., and P. Larkin (2001), Drainage evolution in south-central Africa since the breakup of Gondwana, *South African Journal of Geology*, 104, 47-68.
- Mosley-Bufford, K., E. A. Atekwana., M. G. Abdelsalam, E. Shemang, E. A. Atekwana, K. Mickus, M. Moidaki, M. P. Modisi, L. Molwalefhe (2012), Geometry and faults tectonic activity of the Okavango Rift Zone, Botswana Evidence from magnetotelluric and electrical resistivity tomography imaging, *Journal of African Earth Sciences*, 65, 61-71.
- Mulibo, M. D. and A. A. Nyblade (2013), Mantle transition zone thinning beneath eastern Africa; Evidence for a whole mantle superplume structure, *Geophysics Research Letters*, 40, doi: 10.1002/grl.50694.

- Muller, M. R., A. G. Jones, R. L. Evans, S. Evans, C. J. S. Fourie, X. Garcia, A. Mountford, J. E. Spratt, and S. M. Team (2009), Lithospheric structure and diamond prospectivity of the Rehoboth terrane and Western Kaapvaal Craton, Southern Africa: constraints from broadband magnetotellurics, *Lithos*, 112, 93–105.
- Nair, K. S., S. G. Gao, K. H. Liu, and P. G. Silver (2006), Southern African crustal evolution and composition: Constraints from receiver function studies, *Journal of Geophysical Research*, 111, 111- 117.
- Nguuri, T. K., J. Gore, D. E. James, S. J. Webb, C. Wright, T. G. Zengeni, O. Gwavava, J. A. Snoke and K. S., Group (2001), Crustal structure beneath Southern Africa and its implications for the formation and evolution of the Kaapvaal and Zimbabwe cratons. *Geophysical Research Letters*, 28, 2501–2504.
- Okubo, Y., R. J. Graf, R. O. Hansen, K. Ogowa, and H. Tsu (1985), Curie point depth of the island of Kyushu and surrounding areas, Japan, *Geophysics*, 50, 481-494.
- Omenda, P. A. (2010), The geology and geothermal activity of the East Africa Rift. Presented at the short course V on Exploration of Geothermal Reseource organized by UNU-TGP, GDC and Ken Gen, at Lake Bogoria and Lake Naivasha, Kenya, Oct. 29.

- Ravat, D., A. Pignatelli, I. Nicolosi, and M. Chiappini (2007), A study of spectral methods of estimating the depth to the bottom of magnetic sources from near-surface magnetic anomaly data, *Geophysical Journal International*, 169, 421-434.
- Reeves, C. V. (1972), Rifting in the Kalahari? *Nature*, 237, 95–96.
- Ringrose, S., P. Huntsman-Mapila, A. B. Kampunzu, W. Matheson, W. Downey, B. Vink, C. Coetzee, and C. Vanderpost (2005), Sedimentological and geochemical evidence for palaeo-environmental change in the Makgadikgadi subbasin, in relation to the MOZ rift depression, Botswana. *Palaeogeography, Palaeoclimatology, Palaeoecology*, 217, 265-287.
- Ritter, O., U. Weckmann, T. Vietor and V. Haak (2003), A magnetotelluric study of the Damara belt in Namibia regional scale conductivity anomalies, *Physics Earth and Planetary Interiors*, 138, 71–90.
- Roberts, E. M. N. J. Steven, P. M. O'Connor, P. H. G. M. Dirks, M. D. Gottfried, W. C. Clyde, R. A. Armstrong, A. I. S. Kemp and S. Hemming (2012), Initiation of the Western Branch of the East African Rift coeval with Eastern Branch, *Nature Geoscience*, 5, 289-294.
- Scholz, C. H., T. A. Koczyński and D.G. Hutchins (1976), Evidence for incipient rifting in Southern Africa, *Geophysical Journal of the Royal Astronomical Society*, 44, 135–144.

- Shemang, E. M. and L. N. Molwalefhe (2009), DC resistivity and seismic refraction survey across the SE margin of Lake Ngami, NW Botswana, *Acta Geophysica*, 57, 728 – 742.
- Singletary, S J., R. E. Hanson, M. W. Martin, J. L., Crowley, S A., Bowring, R M., Key, L. V., Ramokate, B B., Direng and M. A., Krol (2003), Geochronology of basement rocks in the Kalahari Desert, Botswana, and implications for regional Proterozoic tectonics, *Precambrian Research*, 121, 47-71.
- Spector, A. and F. Grant (1970), Statistical models for interpreting aeromagnetic data, *Geophysics*, 35, 293–302.
- Tanaka, A., Y. Okubo and O. Matsubayashi (1999), Curie point depth based on spectrum analysis of the magnetic anomaly data in East and Southeast Asia, *Tectonophysics*, 306, 461-470.
- Tselentis, G. A., J. Drakopoulos and K. Dimtriads (1988), A spectral approach to moho depths estimation from gravity measurement in Epirus (NW Greece), *Journal of Physical Earth*. 36, 255-266.
- van Wijk, J., J. van Hunen and S. Goes (2008), Small-scale convection during continental rifting; evidence from Rio Grande Rift, *Geology*, 36, 575-578.

- Whaler, K. A., and S. Hautot (2006), The electrical resistivity of the crust beneath the northern Main Ethiopian Rift, in The Afar Volcanic Province Within the East African Rift System, *Geological Society Special Publication*, 259, 293–306.
- Wölbern, I., G. Rumpker, K. Link, and F. Sodoudi (2012), Melt infiltration of the lower lithosphere beneath the Tanzania craton and the Albertine rift inferred from S receiver functions, *Geochemistry Geophysics Geosystems*, 13, 1- 20.
- Yu, Y., C.A. Reed, S.S. Gao, K.H. Liu, B. Massinque, H. Mdala, M. Moidaki, D. Mutamin, E. A. Atekwana, S. Ingate and M. Ruesch (2013), Crustal and mantle structure and anisotropy beneath the incipient segments of the East African Rift System: Preliminary results from the ongoing SAFARI, *2013 Annual Fall AGU Meeting*.

APPENDICES

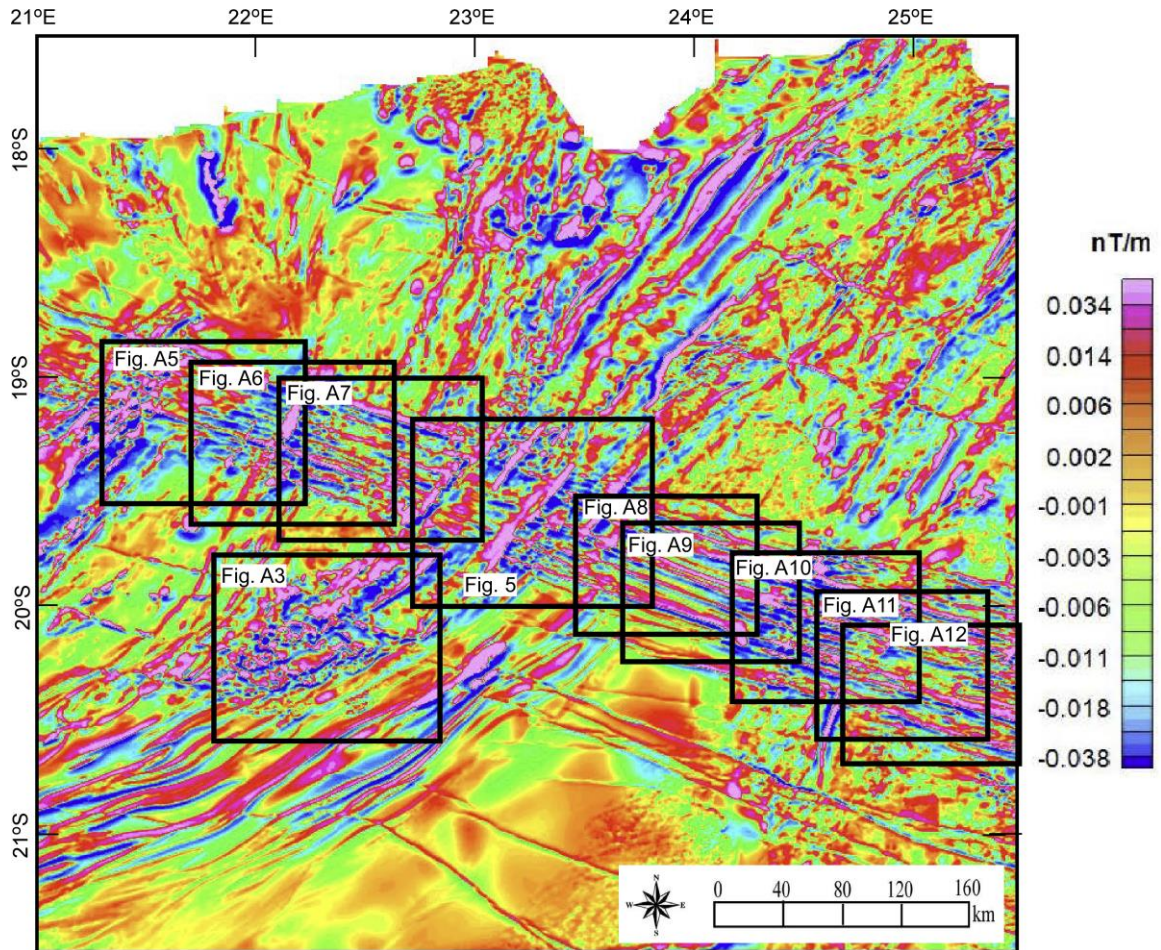


Figure A1. Aeromagnetic anomaly map showing location for 3D inversion blocks presented as figure A3, A4, A5, A6, A6, A7, A9, A10, A11 and A12

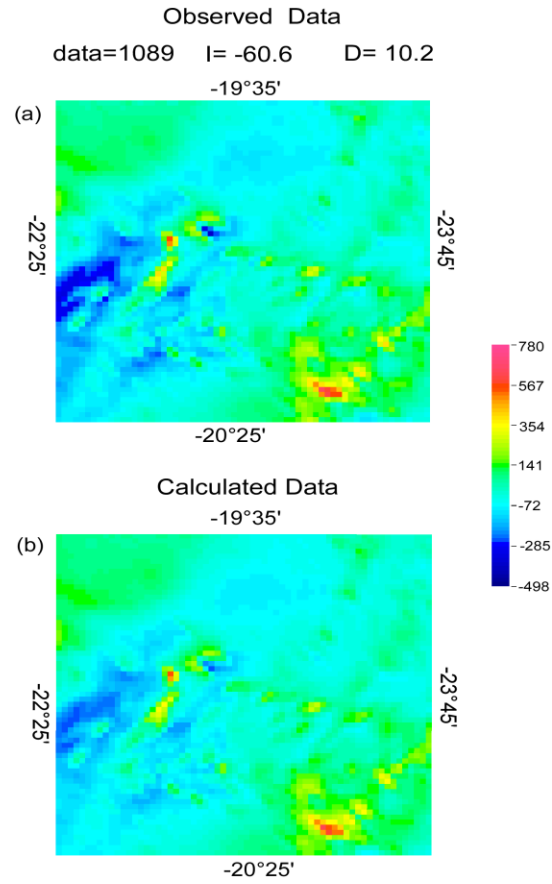


Figure A2. (a) The observed magnetic anomaly map. (b) The Calculated magnetic anomaly map of model in Figure 5a.

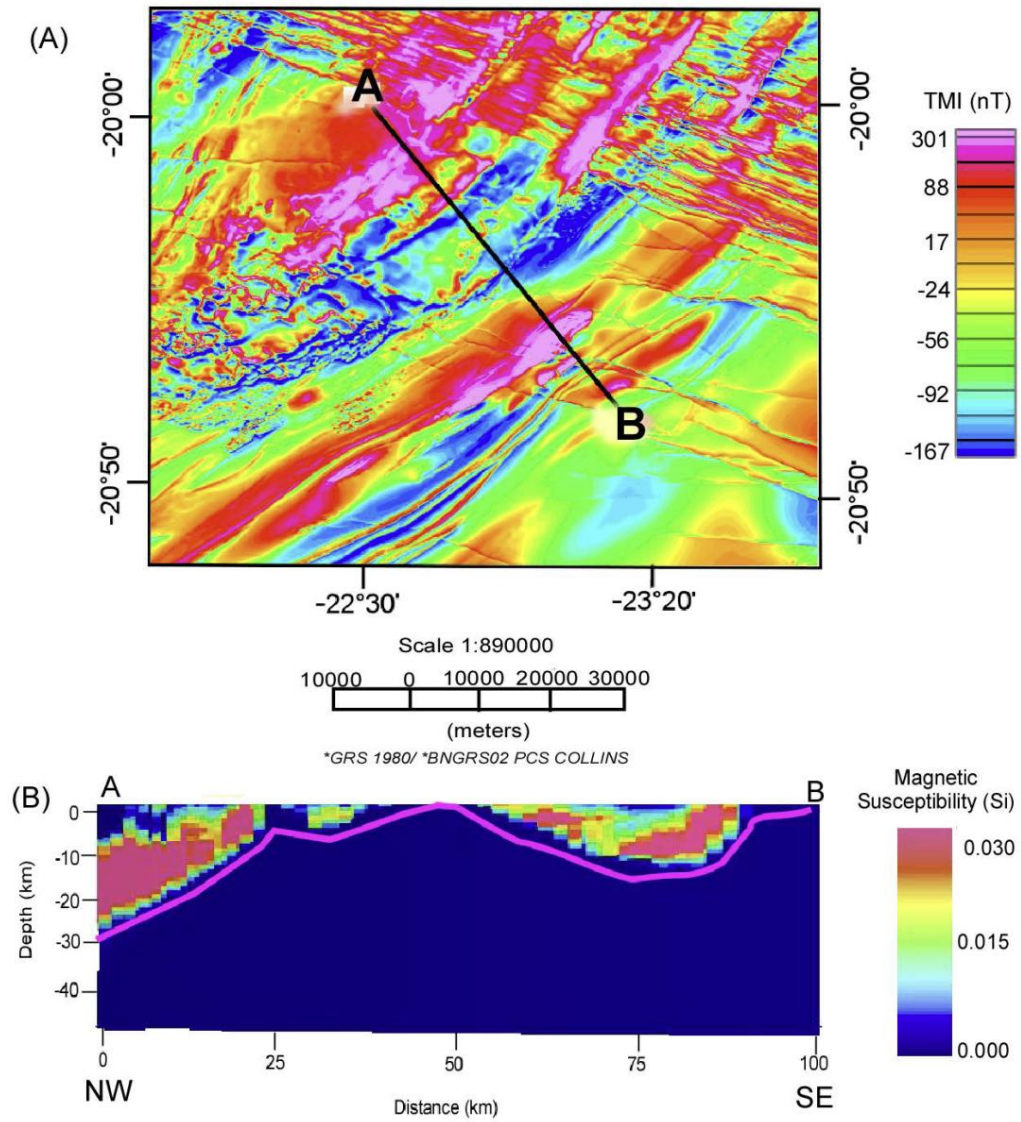


Figure A3. (A) The Magnetic anomalies inverted to produce (B) are the 3D inversion models respectively. The pink line is the base of magnetic sources crust.

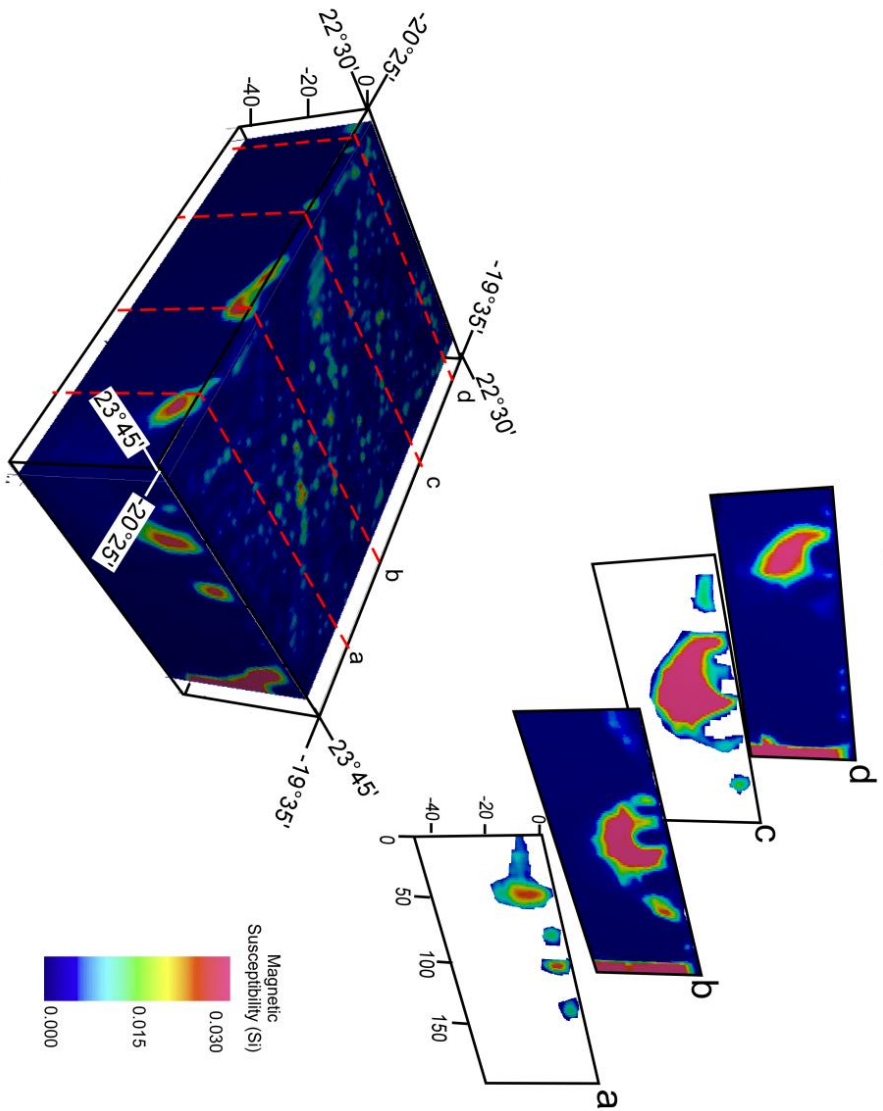


Figure A4. a) An example of $1^\circ \times 1^\circ$ sub-block with ~ 40 depth and E-W depth slices (labeled a, b, c and illustrating the 3D inversion of the aeromagnetic data used for the calculation of Curie point depth.

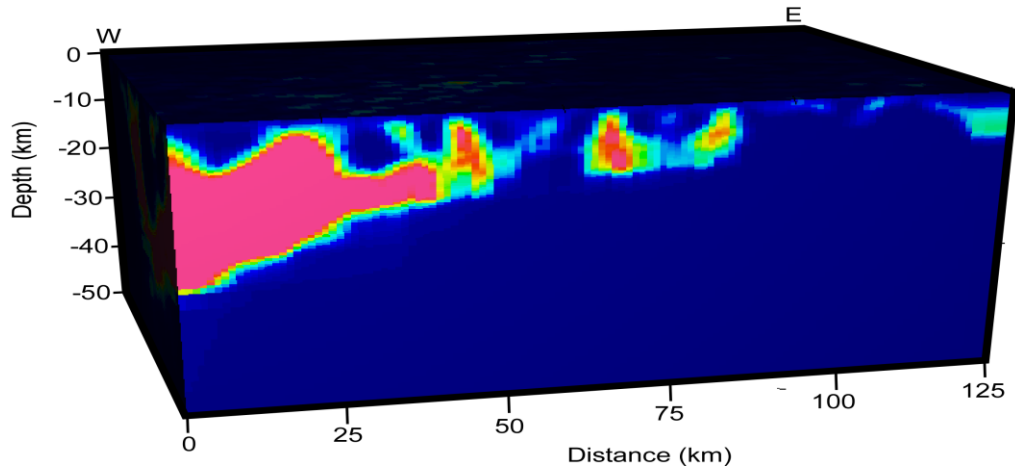


Figure A5. An example of $1^\circ \times 1^\circ$ sub-block with ~ 50 depth showing the 3d inversion below the Congo Craton in the NW side of the rift.

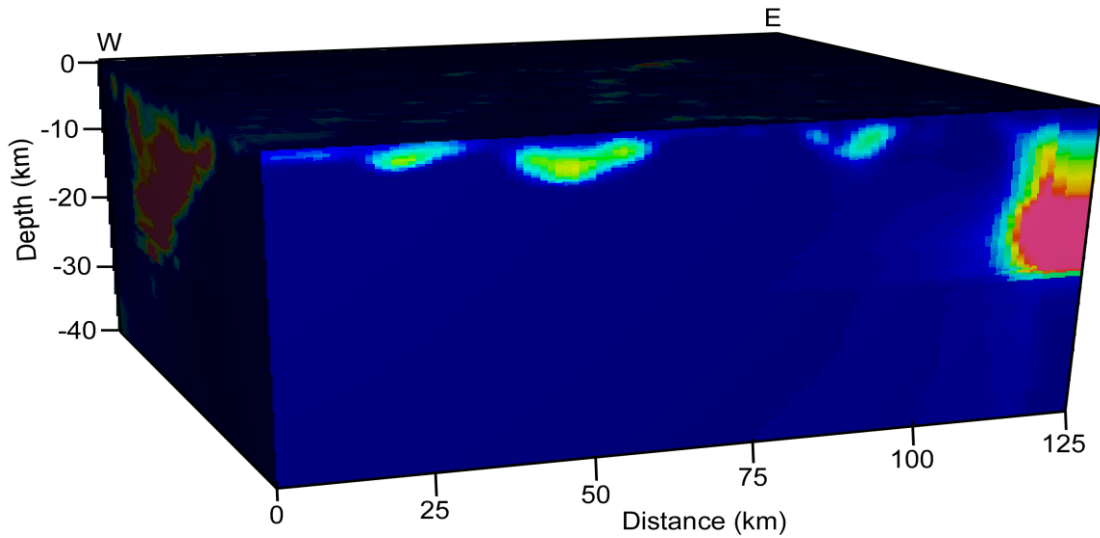


Figure A6. An example of $1^\circ \times 1^\circ$ sub-block with ~ 40 depth showing the CPD below the inverted magnetic anomalies over the SE boundary of the Congo craton (see profile on Figure 5B).

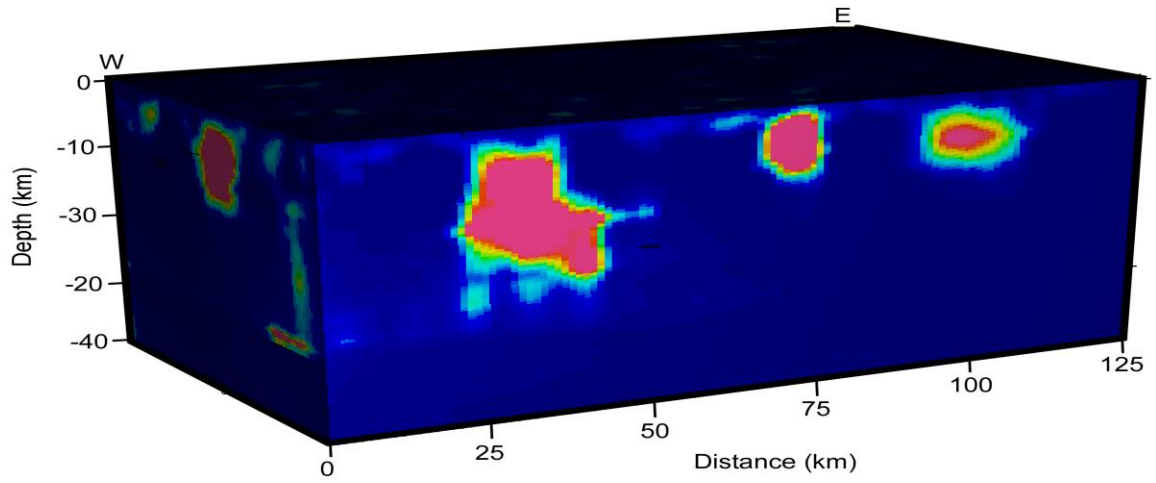


Figure A7. An example of $1^\circ \times 1^\circ$ sub-block with ~ 40 depth between the Gumare Fault and Thamalakane Faults (See Figure 5B for the location).

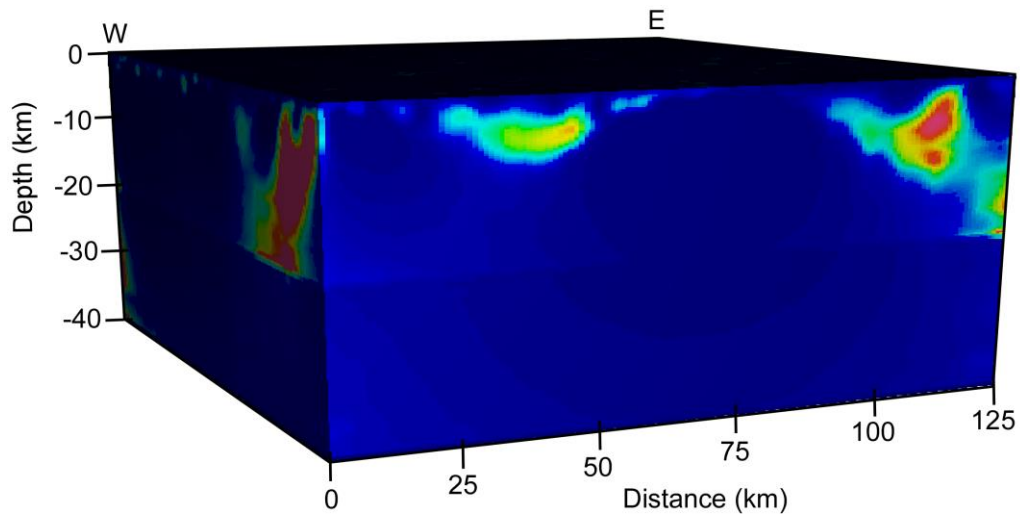


Figure A8. An example of $1^\circ \times 1^\circ$ sub-block with ~ 40 depth between the Tsau fault and the Thamalakane fault (see the Figure 5B cross-section for the location).

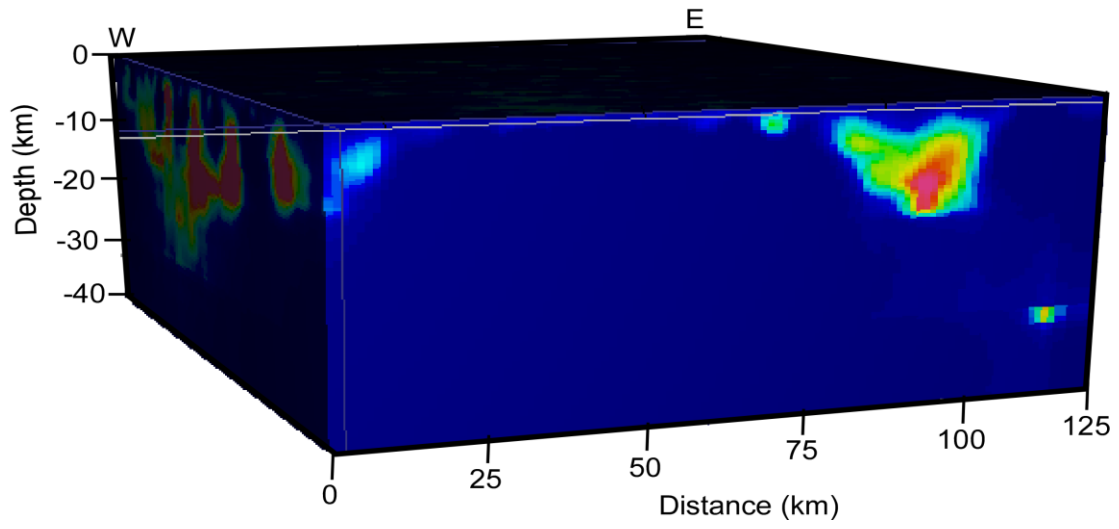


Figure A9. An example of $1^\circ \times 1^\circ$ sub-block with ~ 40 depth model to the southeastern side of the rift and the Damara-Ghanzi-Chobe belt (see Figure 5B for location)

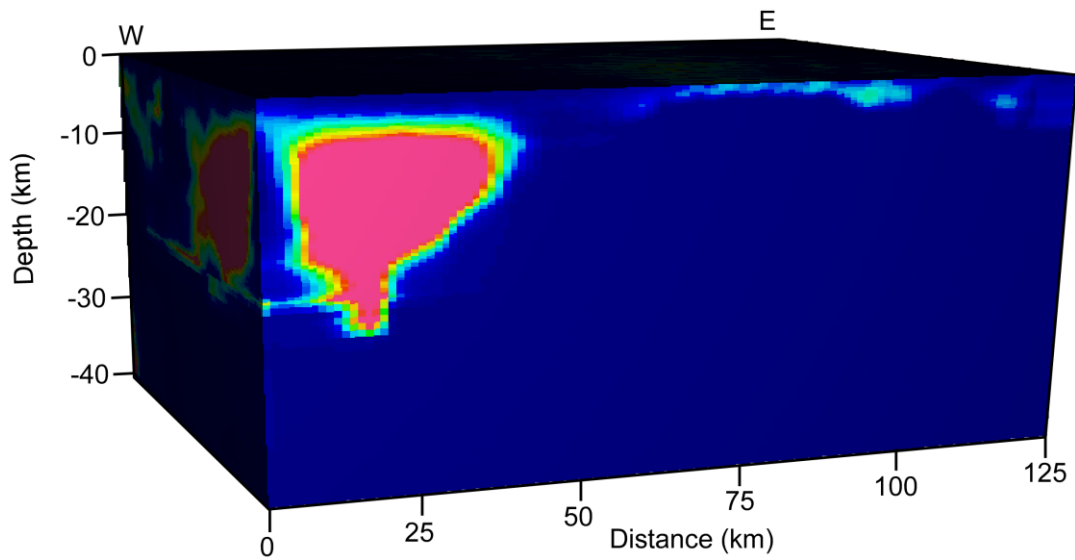


Figure A10. An example of $1^\circ \times 1^\circ$ sub-block with ~ 40 depth of the Kalahari Shear Zone (See Figure 5B for location)

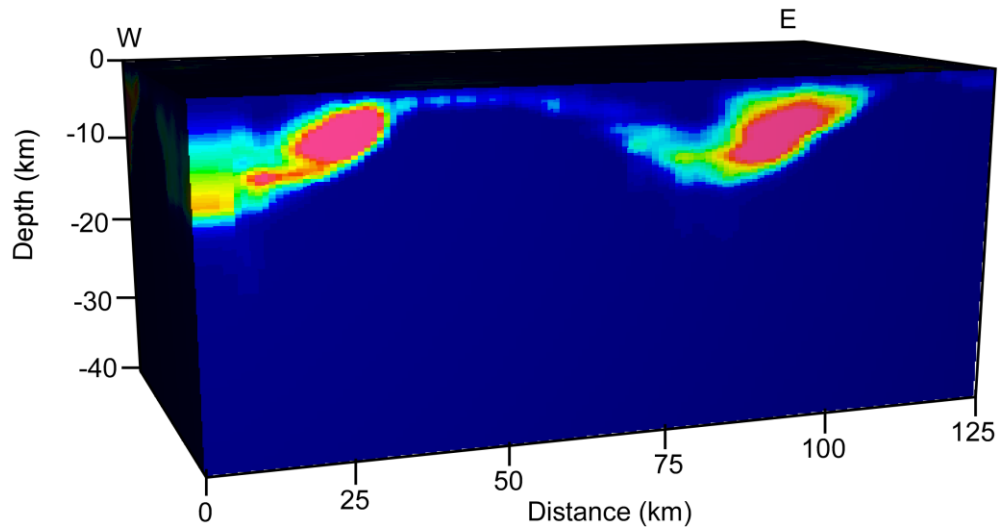


Figure A11. An example of $1^\circ \times 1^\circ$ sub-block with ~ 40 depth on the southeastern boundary of Kalahari Shear Zone, (refer to cross-section A-B in Figure 5B).

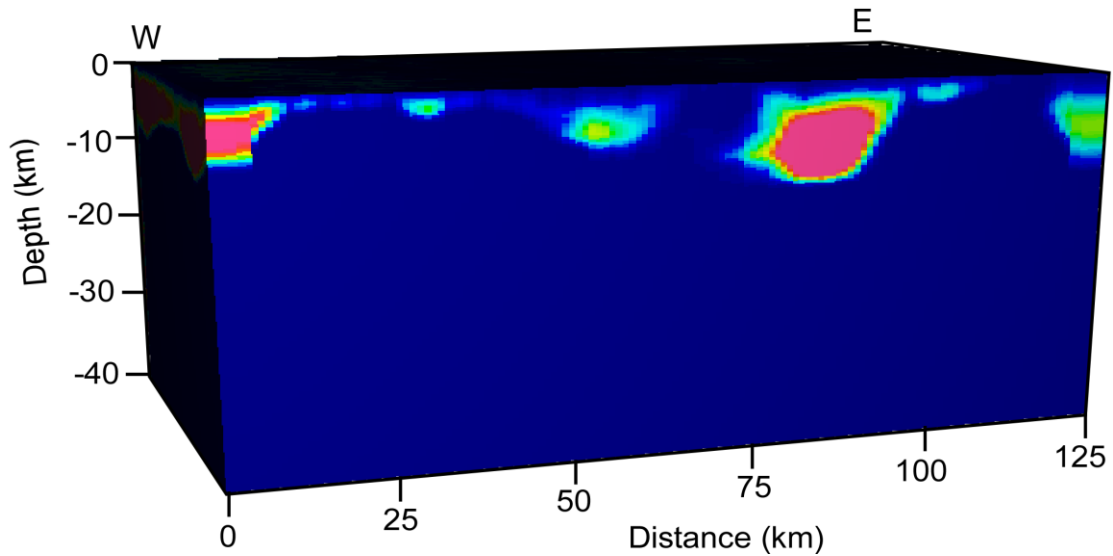
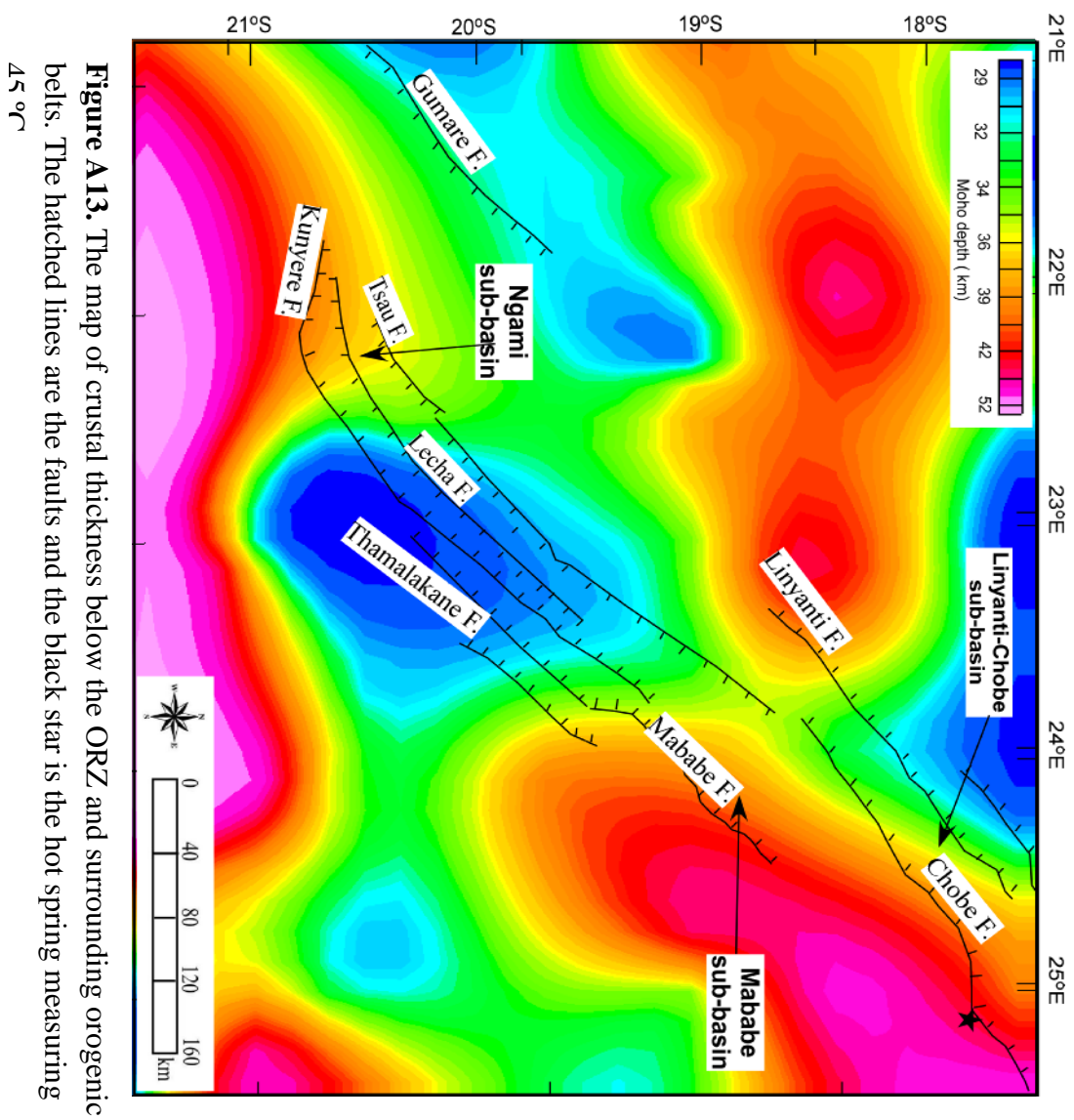


Figure A12. An example of $1^\circ \times 1^\circ$ sub-block with ~ 40 depth of the northwestern side of Mangondi belt along profile A-B on Figure 5B.



VITA

KHUMO LESEANE

Candidate for the Degree of

Master of Science

Thesis: THERMAL PERTURBATIONS BENEATH THE INCIPIENT OKAVANGO
RIFT ZONE, NORTHWEST BOTSWANA

Major Field: Geology

Biographical:

Education:

Completed the requirements for the Master of Science in Geology at Oklahoma
State University, Stillwater, Oklahoma in May, 2014.

Completed the requirements for the Bachelor of Science in Geology at
University of Botswana, Gaborone, Botswana in 2009.

Experience:

Geo-World (TPY) LTD) (Botswana)
University of Botswana (Botswana)

Professional Memberships:

Society of Exploration Geophysics
American Association of Petroleum Geologist
Geological Society of America
University of Botswana Geo Club
Youth Empowerment Sector (Botswana)
Botswana Geologist Association